Determining operating parameters for reverse water gas shift reaction with respect to carbon formation and methantion for syngas production

Karthik Selvam

TU Delft

Determining operating parameters for reverse water gas shift reaction with respect to carbon formation and methantion for syngas production

by

Karthik Selvam

Submitted to obtain the degree of Master of Science, in mechanical engineering,

with the 3ME department, at the Delft University of Technology,

to be defended on August 18, 2022 at 10.00 AM.

Student number :	5264421	
Project duration :	December 21, 2021 – August 18, 2022	
Committee :	Prof. Dr. Ir. Thijs J.H Vlugt,	TU Delft, Supervisor
	Ir. Jan-Jaap Riegman,	T.EN Nethalands B.V, Supervisor
	Dr. H. Burak Eral,	TU Delft
	Dr. Mahindar Ramdin	TU Delft

The work in the thesis was made in collaboration with T.EN Netherlands,

Hydrogen and Syngas Group,
Product Development Department,
T.EN Netherlands, Zoetermeer.

Department of Process and Energy,
Faculty of Mechanical Engineering,
Delft University of Technology.

Acknowledgement

It wouldn't have been possible to write this master's thesis without the help and support of the kind people around me, to only some of whom it is possile to give particular mention here.

First and foremost I would like to express my sincere gratitude to Technip Energies, Netherlands for giving me this challenge right after my internship in their organization. Many thanks to my daily supervisor in the company, Ir. Jan-Jaap Riegman for his guidance, support and his patience for educating me on engineering chemistry not to mentione his unsurpassed knowledge on syngas and hydrogen production technologies. I would like to extend my gratitude to my principle supervisor, Prof. dr. ir. Thijs Vlugt in TU delft, for taking me under his supervisor and providing me with his valuable and experienced inputs on modelling. Indeed, guiding me though the academic pathway to reach my goal, and the faculty of 3ME for giving me the atmost level of education possible amidst the pandemic.

I would like to acknowledge the motivation from my peer graduate students in TU delft, my department manager Stephane Walspurger, and my collegues in the product development department in Technip energies for creating an atmosphere for me to make mistakes and learn. Also, all the fun lunch strolls around the company and friday evening borrels has given me the perfect start to my career as an engineer.

Last but not the least, I would like to thank my parents for letting me explore my passion for science far from home for which I'm grateful and the endless support of my friends during hardships and personal downfalls.

To questions about my future endeavours from my family, friends and wellwishers. I shall quote Sir Winston Churchhill;

" Now, this is not the end. It is not even the beginning of the end.
But it is, perhaps, the end of the beginning "

Karthik Selvam

Delft, July 2022

Abstract

CO_2 is the major contributor of green houses gases in the atmosphere. Two notable branches that revolutionized the approach toward reducing the CO_2 in the atmosphere are Carbon Capture Storage (CCS) and Carbon Capture Utilization (CCU) [8]. CCS has its shortcomings in the long run, a study from MIT shows that the united states have an adequate land area to store CO_2 for 100 years [64]. The important question is, what about after 100 years? The need for efficient methods to utilize the stored or captured CO_2 is a reasonable solution; therefore successful development of efficient methods in utilizing CO_2 is the need for the hour. This work comprises of using reverse water gas shift that utilizes CO_2 as raw material and H_2 produced via electrolysis using renewable electricity from wind or solar energy to produce syngas replacing gasifiation of coal or natural gas that produces CO_2. Syngas is a major raw material for producing useful chemicals such as methanol, dimethyl ether, acetic acid, hydrocarbons and other valuable chemicals [11].

On this wide field of syngas production technology, this work aims in determining the optimal operating condition of the reverse water gas shift reactor to produce hydrocarbons. Hydrocarbon heavier than C_{5+} are used to produce liquid fuels, reverse water gas shift reaction followed by Fischer Tropsch (FT) synthesis is utilized to achive liquid fuels. FT synthesis requires a particular composition of syngas for effective operation and high selectivity. The challenges faced are side reactions such as boudouard and CO hydrogenation that produces carbon and methane in the reactor that are undesired. Carbon deactivates the catalyst and carburization causes ineffective conversion of CO_2 resulting in high operational costs. Methane is hazardous side product that needs to be minimized in the outlet stream of the reverse water gas shift reactor before feeding the same stream into the fischer tropsch reactor.

Less to no literatures are available on reverse water gas shift with respect to carbon formation and methantion for downstream liquid fuel production. The above mentioned objective is countered by modelling a plug flow tubular reactor. A nickel on calium alumina catalyst is used in the reactor. The model is used to determine the operating conditions for the reverse water gas shift reactor to minimize carbon formation and methanation in the reactor. The parameters such as inlet conditions, pressure, inlet temperature, heat input to the reactor are all determined for a desired syngas composition, with no carbon formation inside the reactor and minimum methane in the reverse water gas shift reactor outlet. As a result, carbon activity or potential to form carbon reduced to negligible amount with desired outlet syngas composition of 1.8 – 2.15 and minimum methane composition less than 5 % of the outlet stream. Additionally effects of recycles are analysed and adding H_2O in found to reduced carbon formation at the inlet. At the end of the work detailed summary of operating conditions to effectively operate the reactor without undesired side products are proposed.

Content

List of Figures

List of Table

Nomencleture

$A_{m,\mathrm{ext}}$	Specific internal surface area	$\mathrm{m^2\ kg^{-1}}$
C	Gas phase bulk concentration	$\mathrm{mol\ m^3}$
C_p	Specific heat at constant pressure	$\mathrm{J\ mol^{-1}K^{-1}}$
d	diameter	m
D	diffusion coefficient	$\mathrm{m^2 s^{-1}}$
ΔG	Change in Gibbs free energy	$\mathrm{J\ mol^{-1}}$
E_a	Activation energy	$\mathrm{J\ mol^{-1}}$
$k_{m,\mathrm{CO}}$	rate constant of CO conversion to CH_4	$\mathrm{m^{1.2}mol^{0.6}kg^{-1}s^{-1}}$
$k_{m,\mathrm{CO_2}}$	rate constant of CO_2 conversion to CO	$\mathrm{m^{1.5}mol^{0.6}kg^{-1}s^{-1}}$
K_c	Equilibrium constant in terms of concentration	–
L_p	Characteristic length of particle	m
m	Mass of catalyst	kg
M	Molecular weight	$\mathrm{kg\ mol^{-1}}$
r'	Reaction rate per unit mass of catalyst	$\mathrm{mol\ kg^{-1}s^{-1}}$
R	Ideal gas constant (8.3142)	$\mathrm{J\ mol^{-1}K^{-1}}$
U	Interstitial fluid velocity	$\mathrm{m\ s^{-1}}$
U_s	Superficial velocity	$\mathrm{m\ s^{-1}}$
z	Length of the reactor	m
U	Overall heat transfer coefficient	$\mathrm{W\ m^{-2}K^{-1}}$

Greek symbols

β	Mass transfer coefficient	$\mathrm{m^2\ s^{-1}}$
η	Particle Effectiveness factor	–
ε_p	Porosity of particle	–
ε_b	Porosity of bed	–
μ	Viscosity	$\mathrm{kg\ m^{-1}\ s^{-1}}$
ρ_b	Bulk density	$\mathrm{kg\ m^{-3}}$
ρ_p	Particle density	$\mathrm{kg\ m^{-3}}$
ν	Kinematic viscosity	$\mathrm{m^2\ s^{-1}}$

τ_p	Particle tortuosity	–
ϕ	Thiele modulus	–

Subscripts

0	Inlet
b	Reactor bed
cat	Catalyst
eq	Equilibrium
eff	Effective
i	Species i
in	Inlet of reactor
knu	Knudsen diffusion
m	Related to mass
mol	Related to mole
mol	Related to molecule
out	Outlet of reactor
p	Catalyst particle
s	Related to surface

Dimensionless numbers

Nu	Nusselt number
Pr	Prandtl number
Re	Reynolds number
Sc	Schmidt number
Sh	Sherwood number

Introduction | 1

1.1 The climate is changing so should we

CO_2 emission into the atmosphere has steadily increased, not even the COVID-19 pandemic has limited the emissions in spite of significant decrease in the use of transportation and industrial slow down [1]. Comparing the Global monitoring laboratory data, the monthly average of CO_2 globally has increased from 411.66 ppm in 2020 to 414.01 ppm in 2021 [2]. The continuous increase in anthropogenic CO_2 and other greenhouse gases (GHG) in 2021 has resulted in 1.1°C warmer than the global baseline temperature in the period of the 19th-century [3]. A single degree rise or a half a degree rise in temperature may look insignificant to a lame man, but the effects like drought, arctic melting, increase in sea level, species loss and change in terrestrial ecosystem are alarming. If the emissions continue to increase steadily between 2030s and 2050s, we can observe a two-degree Celcius or more rise in global temperature [4-6]. A beautiful visualization called the "climatic spiral" that illustrates the temperature raise with respect to time is animated by NASA's Scientific visualization studio and is presented below to outforth the seriousness of the situation. The colour of the rings in the image below is the temperature depiction with blue being cold and red being hot. The animation of the described can be seen here [7]. A steady increase can be observed from 1980 to 2021.

As a result of the climatic goals set during the Paris conference in 2015, numerous norms and standards have been placed to reduce emissions and improve climatic conditions. The main object was to keep the global temperature rise below 2^{o}C and limit it to 1.5^{o}C before the end of 2050. To achieve this goal, carbon dioxide in the atmosphere has to be controlled because it alone occupies about 80% of the total GHG in the atmosphere. Unfortunately, the amount of CO_2 in the atmosphere increases day-by-day due to essential human activities. It is inevitable that atleast certain amount of carbon dioxide will be released to the atmosphere on a regular basis. Therefore, along with controlling the amount of CO_2, methods for utilizing the GHG are required. Two notable branches that revolutionized the approach toward reducing the CO_2 in the atmosphere are Carbon Capture Storage (CCS) and Carbon Capture Utilization (CCU) [8]. Regards to CCS, CO_2 is easy to capture at the source (i.e., Process industries, Cement industry) rather than capturing it from direct atmospheric air, because direct air capture systems are less efficient and under-developed compared to inhouse carbon dioxide separation methods (i.e. Pressure Swing Adsorption). Thus, Carbon capture is a viable option when employed as part of the separation process in industries, the captured CO_2 can be stored underground or in a storage facility rather than being released into the atmosphere. CCS has its

shortcomings in the long run, a study from MIT shows that the united states have an adequate land area to store CO_2 for 100 years [9]. The important question is, what about after 100 years? The need for efficient methods to utilize the stored or captured CO_2 is a reasonable solution; therefore, CCU is a viable long-term solution with continuous improvement toward a carbon-neutral or even carbon-negative society given the successful development of efficient methods in the upcoming decades or sooner.

$$CO_2 + H_2 \leftharpoons CO + H_2O \qquad \Delta_r H^o = 41\ \mathrm{kJ/mol} \tag{1}$$

A crucial CO_2 utilization method is converting CO_2 directly to CO via the Reverse water gas shift (RWGS) reaction (Eq.1). RWGS can produce CO and H_2O as its products, the ability of RWGS to produce syngas using CO_2, renewable H_2 and Electricity makes it a very viable option for CO_2 utilization sustainabily. Some of the proven ways of producing renewable-H_2 required for RWGS are biomass or Electrolysis powered by wind energy. Other novice production routes include H_2 production from cyanobacteria and many more that are under research. The produced syngas coupled with renewable H_2 and a successful syngas-conversion technology (Fig.2) provides the potential to produce valuable chemicals and fuels. Some of the valuable chemicals that use syngas as feedstock are Methanol, Ethanol, Dimethyl ether, Acetic acid etc [11]. The more interesting area of research is the production of fuels or liquid hydrocarbons from syngas using CO_2 since most of the feedstock for producing fuels is from the gasification of coal or natural gas that, produces CO_2. Mitigating these sources due to energy transition and depletion of the aforementioned conventional resources has made RWGS a source for syngas. Also, RWGS is an intermediate step in producing heavier hydrocarbons (C_{4+}) via Fischer Tropsch (FT) synthesis (Eq. 2) [63].

$$(2n+1)\,H_2 + n\,CO \longrightarrow C_n H_{2n+2} + n\,H_2O \qquad \Delta_r H^o = -165\mathrm{kJ/mol_{CO}} \tag{2}$$

RWGS is crucial in producing heavier hydrocarbons because they are difficult to produce via direct methods (without RWGS), thus making indirect methods attractive to produce CO and convert them into valuable products to attain high selectivity towards heavier hydrocarbons, i.e., transport fuel. This continuous utilization method replaces fossil fuel with renewable energy, especially in the Gas-to-liquid (GTL) sector [10]. RWGS is also well researched due to its application in space exploration which is key in the future. The water electrolysis system can provide oxygen for breathing or as an oxidizer for impulse fuel produced via the Fischer-Tropsch route [53]. Therefore RWGS catalysis is a vital part of producing synthetic fuel therefore, RWGS is studied in detail in the upcoming chapter.

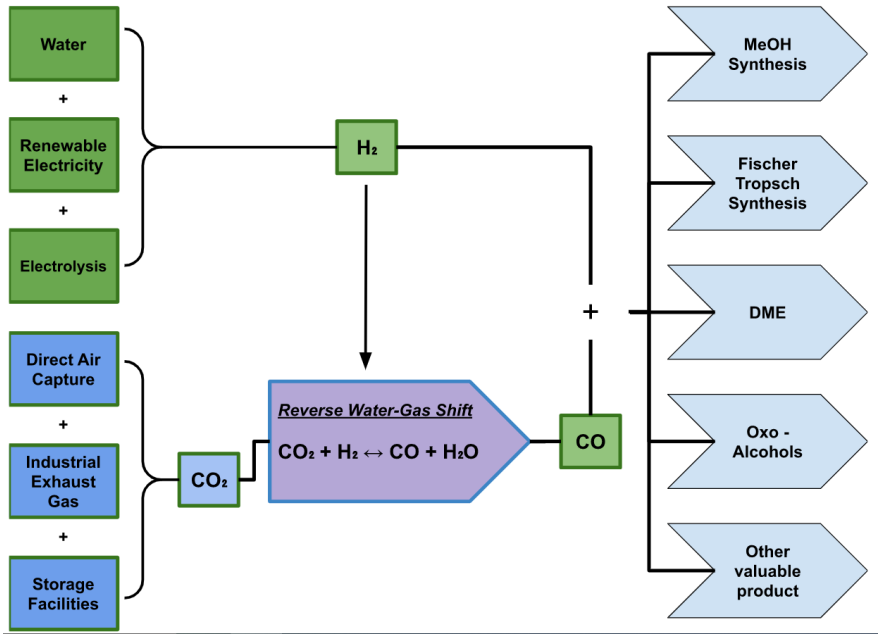

Fig. 1 The simplified flow chart for producing valuable products like Synthetic fuels, Dimethyl ether (DME), Oxo-Alcohols from RWGS as an intermediate; using renewable electricity and CO_2 from industries. RWGS replaces the CO_2 producing processes like coal gasification for a more renewable way to produce syngas.

1.2 State-of-the-art

RWGS catalysis at higher temperature (>450^{o}C) has been a consistent option when compared to photocatalysis or solar thermochemical cycles because they have either a low rate of conversion or require high investment cost [12] in the aspect of producing liquid fuels. On the other hand, electrochemical reduction of CO_2 to valuable products is an active topic under research. However, the feasibility of large-scale use depends on the successful conversion technologies that are still under development for large-scale use or commercialization. Alternatively, the syngas produced via RWGS (Fig.2) can be converted to hydrocarbon via the Fischer-Tropsch process efficiently. Also, the highest volumetric energy density of liquid hydrocarbons compared to liquid hydrogen or methane, enables it to be used as a transport fuel in the existing infrastructure [13].

Currently, most of the focus in the field of CO_2 utilization falls on the development an active, selective, and stable catalysts for the electrochemical and thermal reduction of CO_2. This research focuses on the thermal reduction of CO_2 and thermal reduction produces three main base products, i.e., CO, methanol, and hydrocarbons. The production of CO provides high flexibility since MeOH, and other chemicals can be produced downstream via FT or MeOH synthesis. To obtain high-quality products the indirect method is used i.e. RWGS to produce CO and then followed by FT synthesis. Although recent research on direct FT synthesis is intensifying it is not preferred to produce heavier hydrocarbons. The direct method uses a single reactor with carbon dioxide as its feed, the reactor combines both RWGS and FT reactions to produce lighter hydrocarbons. The

overall reaction is exothermic, providing an energy advantage over RWGS, but designing a catalyst with water resistance and high selectivity of olefins selectivity is challenging.

Water-gas shift (WGS) reaction has been used for decades to adjust the CO:H_2 ratio for a syngas feed from conventional resources for FT synthesis. RWGS is yet to be industrialized; the catalyst and operating conditions optimization are in need for effective performance and large-scale technical applications. The kinds of literature that propose RWGS as a source of syngas for liquid hydrocarbon production always mentioned the effects of side reactions in the RWGS reactor [12,16,19,20,21]. It is imperative to suppress or minimize the production of undesired products from the side reactions in the reactor. Since the outlet feed composition of the RWGS reactor is crucial for an effective FT synthesis to produce high-quality hydrocarbons. Unfortunately, only extensive studies on similar side reactions are performed on Steam Methane Reforming (SMR) (Eq.9) for production of H_2 [18,21]. Scarce to little research is performed with respect to thermodynamic analysis, operating condition and feed parameters to avoid the side reaction on RWGS. Additionally, the side reaction not only produces undesired side products by also causes carbon formation, that leads to the deactivation of catalyst particles in the bed resulting in a buildup of reactor pressure and decreases in heat transfer [11]. Methane and carbon formation are the main products of the side reactions via Methanation and Bouduard reactions respectively (Eq. 6 - 11). From observations in the literature, impurities producing side reactions occur in varying operating conditions, so the challenge is to study the effects of operating conditions and identify windows to avoid these side reactions and run the reactor efficiently.

Production of H_2 should be produced using renewable resources to counter carbon emission. But, significant amount of H_2 produced are still via the traditional routes like natural gas reforming, coal gasification because of their low production cost (< 1$/ kg H_2) [56]. Also, steam methane reforming (SMR) as discussed before is the least expensive and most common method of H_2 production (0.75 $/Kg H_2). [57]. Alternatively, state-of-the-art alkaline water electrolysis (Eq. 3) produces renewable hydrogen at an expensive rate of 2 – 3 $/ kg H_2. At a 0.05 $/kWh electricity cost, if the electricity is from a renewable source the hydrogen produced is carbon neutral. Other recent water electrolysis includes polymer electrolyte membranes (PEM), Solid oxide electrolyzes (SOEC), and carbon-assisted water electrolysis (CAWE), a few of these are still in the research phase. The current state of the art does not allow a cost-effective operation of high-temperature Electrolysis (> 4.5 $/ kg H_2)[56].

$$2\,H_2O \longrightarrow O_2 + 2\,H_2 \qquad (3)$$

Syngas producted via RWGS at high temperature primarly uses Ni-based catalyst and it is extensively researched with many combinations of elements and supports [13,14,15]. Methanation has always been prevalent with Ni-based catalysts, therefore decreasing the selectivity of CO. Nobel metals have shown an affinity towards avoiding the formation of CH_4 above 500^{o}C but due to cost factors they are elimated from further

investigation. In 2021 metal oxides are a topic of discussion because of their economic availability and resistance to sintering at high temperatures [14]. Metal oxides, i.e. Perovskite (ABO_3), offer correct thermal stability and structural flexibility [15], but less to no reliable data about such catalyst's kinetics are disclosed in publications.

Literature review | 2

2.1 Thermodynamics of the reaction

The reverse water-gas shifts (RWGS) is an equilibrium reaction (Eq.4) that has been investigated extensively in the past decades with various catalysts for producing feedstocks to FT synthesis renewably. The WGS is used extensively in the past to fine-tune the H_2:CO ratio of syngas to meet downstream process requirements, since the composition of the feed is an essential parameter for the quality of hydrocarbons produced after FT synthesis. [17].

$$CO_2 + H_2 \leftharpoons CO + H_2O \qquad \Delta_r H^o = 41\ \text{kJ/mol} \tag{4}$$

In the presence of a catalyst due to a higher reaction rate, water gas-shift reaction yields a high conversion of CO and stream to CO_2 and H_2 at low temperatures. On the contrary, the RWGS is an endothermic reaction favoured at high temperatures, > 800°C (see Fig.3). Since, CO_2 is highly stable the chemical transformation requires a significant amount of input energy (high temperature), sufficient reaction conditions, and very active catalysts [54]. RWGS involves a positive change in enthalpy, inferring it is an endothermic reaction; therefore, RWGS is favoured in high temperatures. This is also observed, using the equilibrium constant K_p (Eq.5) that is greater than 1 above 800°C. The equilibrium constant K_p a dimensionless number is the ratio of equilibrium partial pressures or concentration of the reactants and product. For RWGS the number of molecules in the reactants and product side are the same, therefore the pressure does not influence the equillibrum, assuming ideal gas. The equilibrium constant provides an understanding of which direction the reaction will proceed.

$$K_p = \left(\frac{p_{CO}\, p_{H_2O}}{p_{CO_2}\, p_{H_2}}\right) \tag{5}$$

The expression for equilibrium constant K_p as a function of temperature for RWGS reaction is given by Twigg [55],

$$K_p = \frac{1}{\exp\left(-0.29353Z^3 + 0.63508\,Z^2 + 4.1778\,Z + 0.31688\right)}$$

Were, $Z = \left(\frac{1000}{T(K)}\right) - 1$

RWGS is thermodynamically favoured at high reaction temperature, so that accelerates the chemical rate according to the Arrhenius equation. Therefore, the reaction is not kinetically limited but is controlled by thermodynamics. The Gibbs free energy of CO_2 (g) is - 392 kJ/mole at 25°C [62], and since the reactant is more stable here than the desirable product CO (g) with Gibbs free energy - 137 kJ/mole at 25°C [62], it is thermodynamically limited and making it inefficient to produce CO. Therefore H_2 is the main reactant in RWGS that reduces the energy gap and makes RWGS feasible.

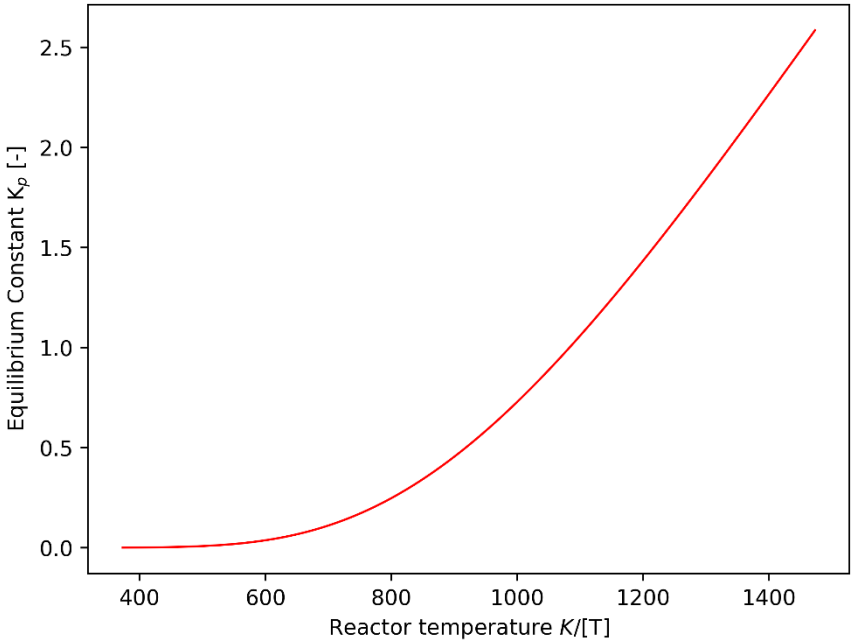

Fig. 2 Equilibrium constant of RWGS at varying temperatures for a equimolar feed. K_p calculated using Eq. 5.

Along with RWGS, there are undesirable side reactions that occur in the reactor that create side products. The unwanted side reaction are listed below with their enthalpy of formation at 25°C [18],

$$CO + H_2 \leftrightharpoons C(g) + H_2O \qquad \Delta_r H^o = -131\ \text{kJ/mol} \qquad (6)$$

$$2CO \leftrightharpoons C(g) + CO_2 \qquad \Delta_r H^o = -172.4\ \text{kJ/mol} \qquad (7)$$

$$CO_2 + 2H_2 \leftrightharpoons C(g) + 2H_2O \qquad \Delta_r H^o = -90\ \text{kJ/mol} \qquad (8)$$

$$CO_2 + 4H_2 \leftrightharpoons CH_4 + 2H_2O \qquad \Delta_r H^o = -165\ \text{kJ/mol} \qquad (9)$$

$$CO + 3H_2 \leftrightharpoons CH_4 + H_2O \qquad \Delta_r H^o = -206.2\ \text{kJ/mol} \qquad (10)$$

$$CH_4 \leftrightharpoons C(g) + 2H_2 \qquad \Delta_r H^o = 74.9\ \text{kJ/mol} \qquad (11)$$

These reactions form two main unwanted side products, carbon and methane. Most of the side reactions are favoured thermodynamically at lower temperatures (<450°C) [18]. A similar trend was observed in other works where carbon formation and methane composition were significantly higher at low temperatures [16,19,20,21]. Adelung et al. point out a similar agreement that, Bouduard (Eq.7) and CO hydrogenation

(Eq.6) are critical for carbon formation at low temperatures < 400°C, and the local concentration and temperature may also cause carbon formation in the reactor [16].

Methanation is favoured thermodynamically at lower temperatures < 600°C [20]; thus, the susceptibility to form methane is prominent at the reactor's outlet, since the outlet temperature is low compared to inside the reactor. Therefore a high outlet temperature of the feed is required to avoid methanation at the feed outlet.

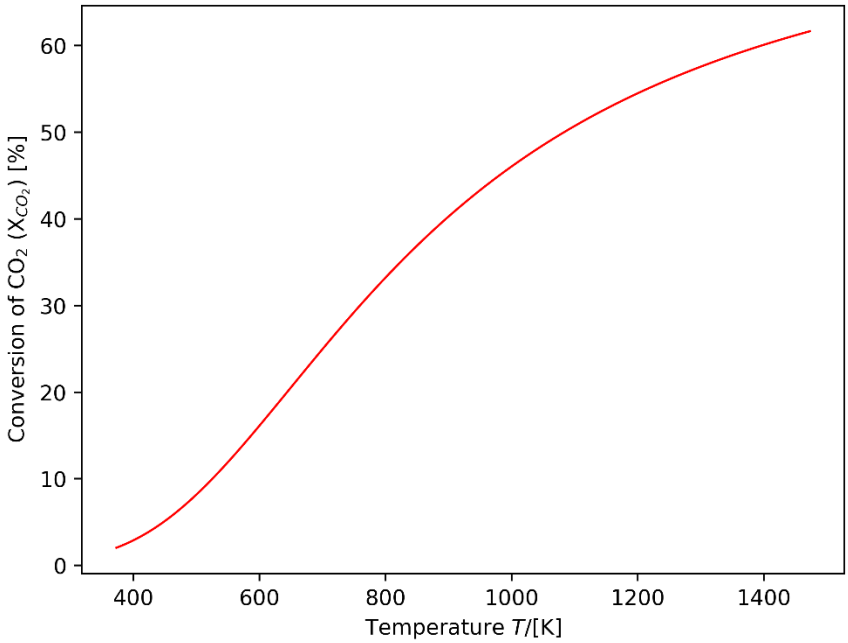

Fig. 3 Equilibrium conversion of CO_2 at varying temperatures for feed composition H_2:CO_2 =1 & 1 bar. The conversion is calculated from the equilibrium constant, using the extent of reaction method.

The equilibrium calculation explains an attainable equilibrium conversion of CO_2 (Fig.4) for an equimolar feed composition at 1 bar and varying temperatures. A thermodynamic equilibrium analysis on RWGS and side reaction is carried out using the Gibbs minimization method for multiple reaction systems to understand the influence of the methanation in the reaction system. Since we operate at significantly high temperatures, we assume ideal gas behaviour. The system incorporates an atomic mass balance, i.e., moles of individual species at inlet conditions equal the moles of individual species at the outlet.

$$n_{\text{carbon,in}} = n_{\text{carbon,out}} \quad (12)$$

Similarly, for hydrogen and oxygen. Total Gibbs free energy in the differential form given as,

$$\mathrm{d}G = -S\,\mathrm{d}T + V\,\mathrm{d}p + \sum_{i=1}^{\mathrm{N}} \mathrm{d}n_i\,\mu_i \quad (13)$$

Where S is the system entropy, T is the system temperature, V is the system volume, P is the system pressure, n_i is the stoichiometric coefficients of component i, and μ_i is the chemical potential of component i. As total Gibbs free energy is calculated in an isolated system for a given temperature and pressure, the total Gibbs free energy is expressed as,

$$G = \sum_{i=1}^{N} n_i \, \mu_i \qquad (14)$$

Expanding the chemical potential and substituting the fugacity (f) for the ideal mixture, the Gibbs energy is minimized using the Sequential Least squares programming in python with the atomic mass balance as constraining. The equilibrium compositions of the components are obtained, the result is plotted below (Fig.5) to understand the equilibrium compositions.

$$G = \sum_{i=1}^{N} n_i \, (G_{f,i}^{o} + RT \ln \frac{f_i}{f_i^{o}}) \qquad (15)$$

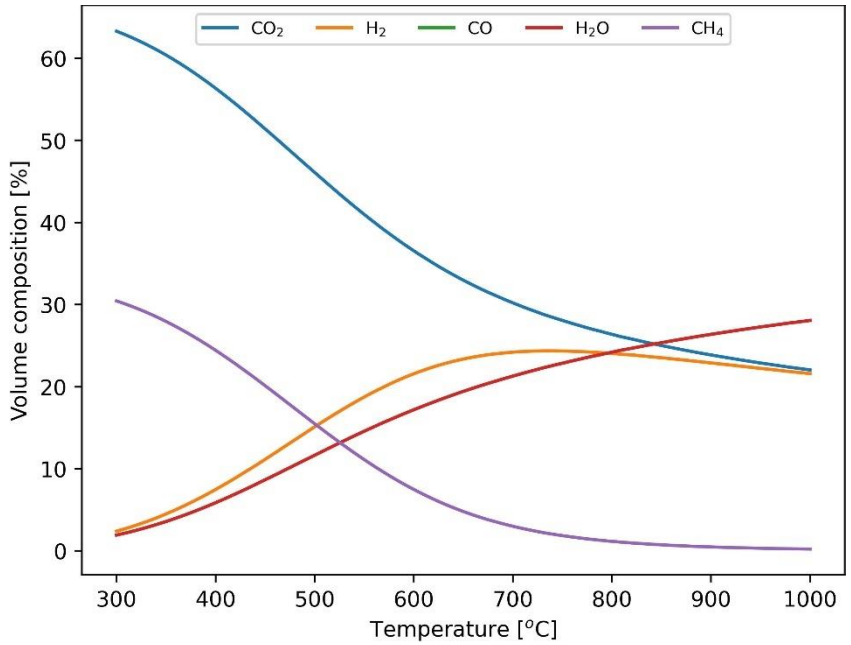

Fig. 4 Equilibrium composition involving RWGS and methanation reactions at H_2/CO_2 = 1 and 1 bar of pressure. It is calculated by using the gibbs minimization method. Methane formation is suppressed or insignificate above 1073 K (800°C)[1] is accordance to litratures.

[1] The composition of CO and H_2O overlaps each other in the figure and similarly therefore not indistinguishable.

2.2 RWGS Catalyst

Catalyst plays a significant part in RWGS; therefore, a short discussion presents the current catalysts trends and research with respect to RWGS catalysts. The catalyst for RWGS should have properties such as high thermal stability since the reactor has to operate at high temperatures for an extended period. Also, high selectivity towards CO formation, since methane and methanol are formed at higher ratios of H_2:CO_2. A plethora of research has been done in the field of heterogeneous catalysts for CO_2 to CO conversion via RWGS. The works are classified chiefly as noble metal and non-noble metal catalysts. Noble metals such as Pt, Rh, Ru are less prone to coke formation and corrosion and display high activity towards H_2 dissociation [23,24]. They show CO_2 conversion close to equilibrium, and the undesired products such as coke and methane are suppressed above 500^{o}C [22]. Unfortunately, their cost and unavailability have forced the development of cheaper alternative non-noble metal catalysts, mainly 3d transition elements, i.e., Au, Pt, Rh, Pd, Cu, Ni, Fe, Co.

The 3d transition elements produce varying results on different supporting metals structures. The most common supports for RWGS are Al_2O_3, SiO_2, TiO_2, CeO_2, transition metal carbides (TMC), and metal-organic framework (MOF) [22]. Cu is one of the popular catalysts but due to poor thermal stability and a strong tendency to sinter at 300^{o}C, support structures are essential. when supported on CeO_2 or Au nanoparticles, they provide high conversion and are close to equilibrium with 100% selectivity towards CO. However, sintering and fast deactivation arise as a problem in the long run [25]. Pt works well on La-ZrO_2 support with increased CO_2 conversion as compared to Fe or Cu, but the low selectivity of CO has influenced its usage [26].

Ni-based catalysts perform well at relatively high temperatures > 500^{o}C, with a high tendency to form methane at lower temperatures. When added with supports and promotors Ni-based catalysts are suitable for high-temperature RWGS. For example, 3 wt.% Ni/Ce-Zr-O_x is highly stable and enables mitigation of carbon deposition through carbon gasification to maintain stability for a long time even after 80 hours at 50% conversion [27]. Also, adding elements such as Fe increased the activity, stability, and selectivity of Ni/Al_2O_3.

Based on the above discussion and the tabulation below, Ni-based catalysts work effectively at higher temperatures. Also, a kinetic model is available for a Ni-based catalyst for RWGS at high temperature; therefore, a Ni-based catalyst is chosen for modelling the tubular reactor. A list of the catalyst with their selectivity and conversion towards CO_2 for high temperature application are tabulated below for future reference and usage.

Table 1. List of catalyst applicable for high temperature RWGS catalysis with conversion of CO_2 and selectivity of CO at given feed composition and operating conditions.

Catalyst	**H_2/CO_2**	**Temperature**	**Pressure**	**CO_2 conversion**	**CO selectivity**	**Reference**
Name	-	(°C)	(MPa)	(%)	(%)	
10% Cu/AlO_3	3:1	500	0.1	60	-	[29]
In_2O_3 / CeO_2	1:1	500	-	20	-	[30]
Cu/Zn @C MOF	3:1	500	0.1	5	100	[31]
Ni	4:1	520	-	55	20	[32]
Fe	4:1	540	-	27	84	[32]
$La_{0.75}Sr_{0.25}FeO_3$	1:1	550	0.1	16	95	[12]
PtK/Mullite	1:1	550	0.1	30.9	99	[33]
Ni/CeO_2	1:1	550	-	24	100	[34]
Cu/CeO_2	3:1	600	0.1	50	100	[35]
Cr_2O_3 / Cu	4:1	600	0.1	45	100	[36]
4% Cu-Al_2O_3	2:1	600	0.1	47	100	[14]
1%Cu/ β-Mo_2C	2:1	600	0.1	41	100	[37]
Cu/Al_2O_3	3:1	600	0.1	>50	100	[14]
Pd/SiO_2	1:1	600	0.1	29	82	[38]
Pd-In/SiO2	1:1	600	0.1	10	100	[38]
0.3% Fe/SiO_2	1:1	600	0.1	12	-	[39]
Cu-Fe/SiO_2	1:1	600	0.1	16	-	[40]
$BaZr_{0.8}$ $Y_{0.2}$ $Zn_{0.04}$ O_3	1:1	600	-	27	93	[41]
Fe Oxide NPs β-Mo_2C	1:1	600	-	38	>85	[42]

α–MoC $_{(1-x)}$	4:1	600	-	60	100	[43]
$BaZr_{0.8}Y_{0.16}Zn_{0.04}O_3$	-	600	-	37.5	97	[41]
Fe-Mo-Al_2O_3	1:1	600	0.1	45	100	[44]
Ni/SiO_2	4:1	660	-	64	100	[45]
Ni-K/Al_2O_3	1:1	700	0.1	42	~100	[46]
CuFe/Al_2O_3	1:1	700	-	-	-	[47]
gamma-Al_2O_3	6:1	700	0.1	51	90	[28]
NiO/$Al_{12}O_{19}$	6:1	700	0.1	74.6	75	[28]
Ni/CeO_2	1:1	750	-	42	100	[48]
Ni/CeO	1:1	750	-	47	100	[49]
Ni/CeO_2	4:1	850	-	80	90	[50]
1% Pt/TiO_2	4:1	875	-	48	-	[51]
NiO/ SBA-15	1:1	900	0.1	55	100	[52]

2.3 Catalyst Deactivation

The catalyst deactivation results in an ineffective reaction rate and finally failure of the catalyst. The main deactivation phenomenon, are sintering, poisoning, and coking (fouling). Sintering, also referred to as aging, is the loss of catalytic activity due to a loss of active surface area resulting from prolonged exposure to high temperatures. The active surface area may be lost either by crystal agglomeration and growth of the metals deposited on the support or by narrowing or closing of the pores inside the catalyst. Sintering is irreversible and creates changes in particle size distribution thus impacting the efficiency of the catalysis overall. Secondly, Poisoning is the loss of catalytic activity due to the chemisorption of impurities on active sites. Poisoning may sometimes decrease the activity, or sometimes impurities can enhance selectivity. Sulphur is a commonly observed impurity in many fossils fuel-derived CO_2 feedstock. It is adsorbed on the catalyst's surface and blocks active sites resulting in catalyst deactivation; depending on reaction conditions, adsorber sulphur is destabilized and desorbed as H_2S [58]. Therefore further downstream processes are required to remove these impurities. Thirdly,

coking/fouling this phenomenon is the main cause for catalyst deactivation in RWGS catalysis; thus, its discussed in detail here.

Coking is a physical (mechanical) deposition of species from the fluid phase onto the catalyst surface. This result in activity loss due to blockage of sites or pores. The definition of coke and carbon are somewhat arbitrary and by convention related to their origin. Carbon is typically a product of CO disproportionation (Eq.7), while coke is a product of decomposition or condensation of hydrocarbons on the catalyst surface [59]. Therefore, the forms of deactivation vary depending on operating conditions, and coke formation mechanisms vary with catalyst type. Carbon may, [60]

(1) Chemisorbed strongly as a monolayer or physically absorbed and blocks metal surface with active sites
(2) Encapsulate a metal particle and thereby deactivate the particle
(3) Plug micro pores denying access to the crystallites inside these pores

Since we are using a Ni- based catalyst mechanism of carbon deposition and coke formation on the Ni metal catalyst from CO is given below [59],

$$\mathrm{CO(a)} \longrightarrow C_\alpha(a) + O(a) \quad (16)$$

$$\mathrm{C_\alpha(a)} \longrightarrow C\ in\ Ni \longrightarrow C_v \quad (17)$$

$$\mathrm{C_\alpha(a)} \longrightarrow Ni_3C\ (s) \quad (18)$$

$$\mathrm{C_\alpha(a)} \longrightarrow C_\beta(s) \longrightarrow C_c(s) \quad (19)$$

$$\mathrm{C_\alpha(a) + 4H(a)} \longrightarrow CH_4(g) \quad (20)$$

Where, a, g, s refers to adsorbed, gaseous, and solid states respectively on a metal catalyst,

Table 2. Forms of carbon species formed by the decomposition of CO on Nickel catalyst [59].

Structural type	Designation	Temperature of formation (^oC)
Adsorbed, atomic (surface carbide)	C_α	200-400
Polymeric, amorphous films or filaments	C_β	250-500
Vermicular filaments, fibers, Whiskers	C_v	300-1000
Nickel carbide (bulk)	C_γ	150-250
Graphitic (crystalline) platelets or films	C_c	500-550

Two things are evident from the above discussion, CO is the main source for all types of carbon and carbon formation is temperature-dependent. Since CO is the desired product from RWGS, it is vital to study the effects of CO in catalyst deactivation, via CO disproportionation reactions along with RWGS in the reactor.

2.4 Objectives of study

The goals of this work are :

- Determine the energy required for the tubular reactor for producing syngas via high-temperature RWGS reaction
- Determine reactor operating conditions to produce a suitable outlet composition for downstream FT synthesis with minimum methane to produce hydrocarbons
- Provide a study on operating windows (risk zone) to reduce or eliminate carbon formation to avoid catalyst deactivation
- Provide inputs based on operating conditions determined from the model; to initialize the catalyst test program

2.5 Scope and Plan of action

A possible avenue for sustainable development is the catalytic conversion of CO_2 to liquid fuels by Fischer Tropsch synthesis and solar or wind energy. The reverse water gas shift reaction (RWGS) is the first step. The produced CO is further converted to liquid fuels by Fischer Tropsch synthesis and is more reliable in producing heavier hydrocarbons than the direct method. The conversion of CO_2 and H_2 depends upon several factors such as catalyst selection, the ratio of CO_2: H_2, and reaction temperature and pressure [28]. The conversion is mainly affected due to catalyst deactivation from mechanisms such as sintering and coking of catalyst particles. However, no systematic study is found in the literature on the effects of operating conditions to reduce or avoid Carbon formation on RWGS. Therefore, a 1D tubular reactor model for RWGS and its side reactions is to be modelled. The model includes the kinetics incorporating the internal and external mass transport effects in the catalyst. Then the model is used to determine the various process conditions for RWGS reaction concerning carbon and methane formation and an appropriate solution suitable for downstream FT synthesis is to be determined.

The most available studies of RWGS catalysis are performed at low temperatures, where methane and carbon formation is thermodynamically favoured. This work studies RWGS at high temperatures to obtain CO as the main products by reducing methanation at the reactor outlet and carbon on the catalyst surface. The selection or investigation of viable catalysts are out of bounds for this work; therefore, a kinetic model is chosen for modelling the rector.

The model will simulate a tubular reactor with a Ni-based catalyst. The kinetics for the model is adapted from research in T.EN Netherlands that preceded the current work [20]. The kinetic model used a spherical-shaped catalyst, now its being replaced by a commercially available Raschig ring shape with dimensions 8 x 8 mm (Height x Outer Diameter) and 3 mm hole. The parameters that influence the conversion, such as reaction rate, temperature, reactant concentration, Gas hourly space velocity (GHSV), and feed composition, are varied. By varying the parameters mentioned earlier, optimal operating

conditions are determined for maximum conversion of CO_2 with minimal risk of carbon and methane formations in the reactor.

The outcome of this work is an essential step for the optimization and application of RWGS technology by T.EN Netherlands BV. A better understanding of reaction kinetics, side products, and process parameters can contribute to the optimization of reactor configuration, energy requirements, plant integration for continuous production of valuable chemicals from CO_2.

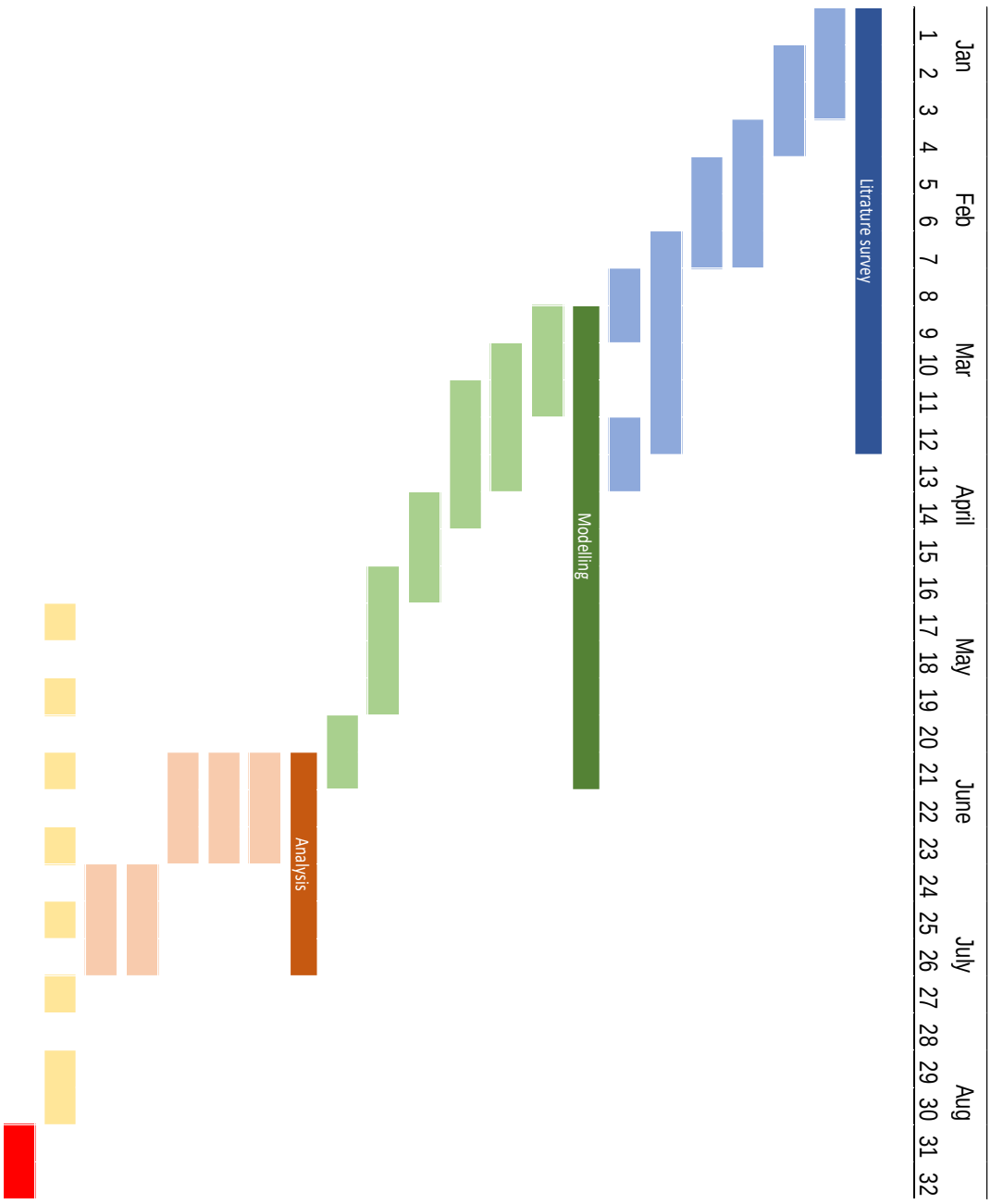

Fig. 5 : Gantt chart for thesis planning and project completion

3 Modelling methodology

This chapter provides an overview of the various models that can be used to describe a fixed bed reactor. Also, the methodology used to model the fixed bed reactor for heterogeneous catalysis. This model will then investigate the operating conditions and their impact on the side reaction.

3.1 Model Overview

There are two types of heterogeneous catalytic reactors. First, reactor where the solid catalyst has a fixed position relative to one another. Second, in reactors where the solid particles are suspended in fluid and constantly move [68]. The first case is ideal for our application because it is simple, well-known, easy to scale up and robust. It is also the case where the mass transfer is moderate compared to a fluidized bed due to diffusion limitations [68,69]. These diffusion limitations are also studied using the model. The packed bed reactor is an assembly of usually uniform-sized catalyst particles arranged randomly and held in place firmly within a tube [68]. The bulk fluid flows through the voids in the catalyst bed and reacts to produce the desired products [72]. Due to the complex physical-chemical phenomenon inside the reactor, describing the exact conditions inside the rector is either impossible or leads to very complex mathematical problems [66]. The precision of the model depends on the effectiveness and accuracy of the parameters that go into the model. Most of the parameters are calculated using empirical or semi-empirical correlations [78]. Therefore, it is concluded that no universal models are used; thus, the description of most reactors relies on creating a model that attends to the most crucial problems at hand.

The models describe a fixed bed reactor are mainly classified as continuum and cell models [69]. In the cell model the reactor is represented by a network of ideally stirred tank reactors (cells). Each cell is connected to its adjacent cell, and the interaction between these cells forms the cell model. The simplest model is obtained by assuming that the network is a one-dimensional series of stirred tanks, where each tank represents one stage of the reactor. The model is equivalent to the finite difference approximation of the one-dimensional pseudo-homogenous model [65,66,67].

The continuum models are the most common and widely used; this model has a heterogeneous system treated as one or multiphase continuum. The continuum approach results in conservation equations for the bulk fluid and solid phase variables [70,71]. The reason to use the continuum approach is that former mass and heat transfer experiments have been analyzed almost exclusively based on continuum models; thus, the parameter values are available for comparison. Furthermore, non-linear reaction rates can be

sometimes handled easier in differential equations. Therefore, a continuum modelling methodology is chosen in this work. In this sense, the model is viewed as a pseudo homogenous or heterogeneous model.

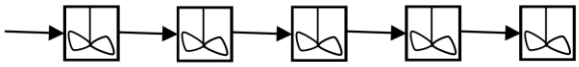

(a)

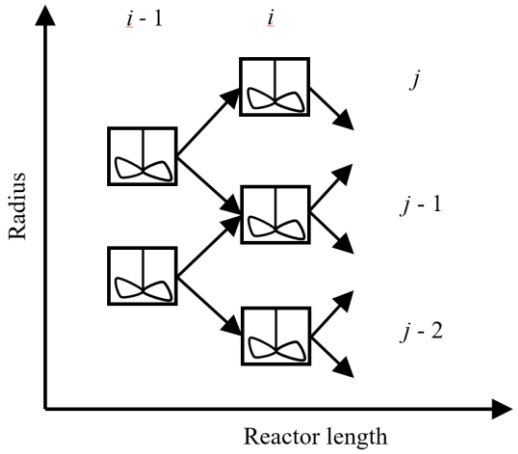

(b)

Fig. 6 (a) One-dimensional series of stirred tanks representing as cell along the length of tubular reactor, multiple stir tanks resembles the catalysis occurring at one part of the tubular reactor then the partically converted reactant are moved to the next reactor and so on along the length of the reactor (b) Two-dimensional cell method with stirred tanks representing the cells along the length represented with coordinate i and the radius of the tubular reactor represented with coordinate j.

The pseudo homogenous models envision that the catalyst surface is exposed to the bulk fluid conditions, i.e., there is no fluid to particle heat and mass transfer resistances. The basic heterogeneous model considers only transport by plug flow but differentiates between bulk fluid and the solid catalyst phases. Therefore, conservation equations for both phases are evaluated to incorporate the heat and mass transfer resistances between the bulk fluid and the solid catalyst. To avoid complexity in the conservative equations and obtain the exact effects of a heterogeneous model, a global reaction rate is introduced. This global or effective reaction rate considers the catalyst's heat and mass transfer limitations that must be incorporated into the homogenous model [68]. This approach has been used in this work because this model is widely employed in the early development stages of reactor design. The 1D model is chosen because it can easily be used to determine the effects of changes in design parameters and operating conditions [68,69], which is the goal of this work. Also, 2D models provide information about radial temperature profiles within the bed. Still, such information is beneficial in evaluating the potential for runaway reactor conditions [68] which is unnecessary in this case of an endothermic reaction.

3.2 Modelling methodology

The complete reactor model consists of two sub-models: the catalyst and tubular models. The catalyst model consists of the kinetic required to calculate the global reaction rate, and the tubular model consists of the fluid properties, conservation equations and operating parameters. Both the models are explained in the forthcoming sections.

3.3 Catalyst model

Understanding the diffusion process in heterogenous catalysis is very important to determine the effectiveness of the catalyst and the overall reaction rate or the global reaction rate. The catalysis occurs between the adsorbed reactants and active sites dispersed throughout the porous structure of the catalyst; therefore, the rate of reaction strongly depends on the accessibility of reactants to those active sites. The diffusion process consists of the following steps:

1. Diffusion of reactant to the external surface of the catalyst from the bulk fluid through the boundary layer of the catalyst.
2. Diffusion of reactant into the porous structure of the catalyst
3. Adsorption of the reactant on the inner surface of the porous catalyst
4. Surface reaction of adsorbed reactant to produce the adsorbed product at the catalyst surface
5. Desorption of product from the inner surface of the porous catalyst
6. Diffusion of formed products through the porous network to the external surface of the catalyst
7. Diffusion of product from the external surface to the bulk fluid through the boundary layer of the catalyst

These results in a concentration gradient in the catalyst pellet and the boundary layer; steps 1,2,6, and 7 are purely physical phenomena compared to the other steps (chemical processes) with strong temperature dependency. If there is resistance to mass transfer from the bulk phase to the external surface area of the particles and the active sites inside the pore, there is an influence on the global reaction rate by mass transfer. Since the model is for a tubular reactor for a lab-scale setup, it is assumed that the catalyst is isothermal and is at the same temperature as the bulk phase of the gas [77]; the temperature gradient in the catalyst is neglected. Thus, only mass transfer is the main influencing factor of the global reaction rate.

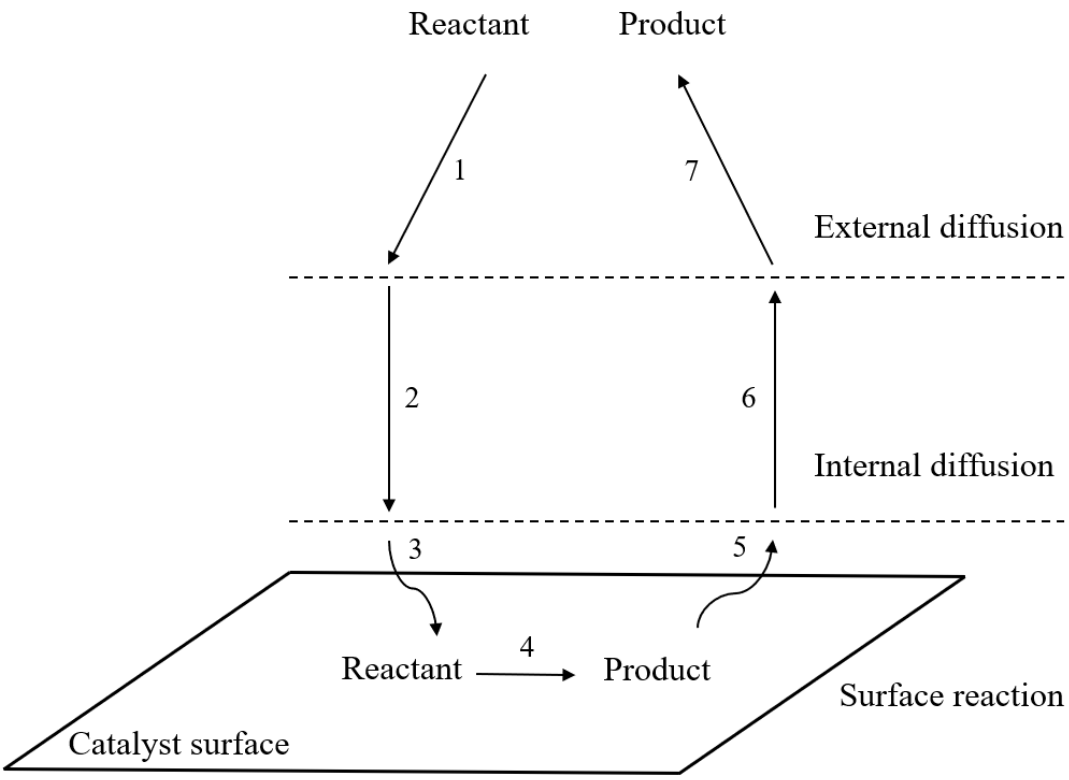

Fig. 7 Elementary steps involved in a heterogenous catalysis, denoting the external diffusion from the bulk of the gas to the external surface of the catalyst (steps 1 & 7) and internal diffusion from the external surface of the catalyst into the porous medium and the activity sites (step 2 & 6), these steps are illustrated to emphasize the impact of mass transfer limitation in heterogenous catalysis.

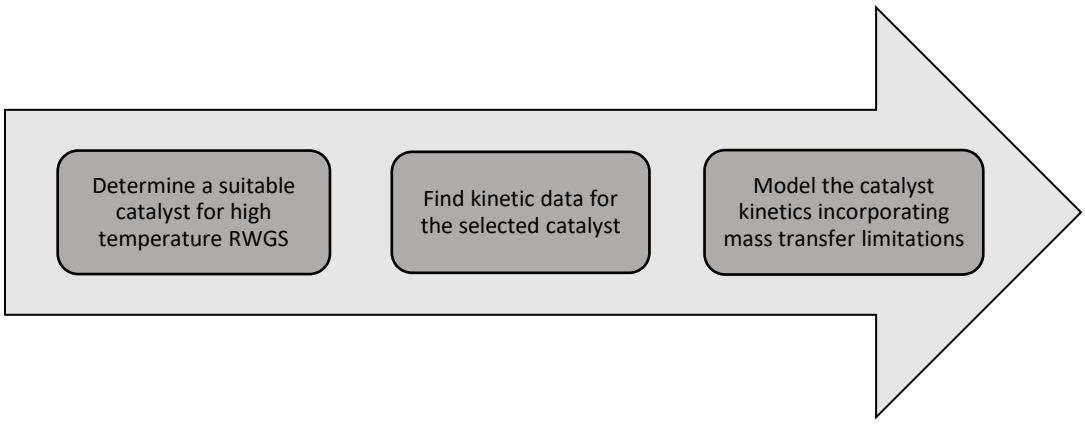

Fig. 8 Flowchart describing the methodology involved in developing the catalyst model by including the kinetics for the Ni on calcium aluminate, then determining the internal and external mass transfer limitations to calculated the effective reaction rate to complete the reactor model.

3.3.1 Influence of mass transfer

There are two classifications of mass transfer in heterogeneous catalysis, external mass transfer (Steps 1,7) and internal mass transfer (steps 2,6). These two phenomena are parameterized and are used to model the global reaction rate.

The first case focuses on internal mass transfer, also known as pore diffusion. The concentration of reactants at the pore entry is much higher than the inside of the pore, and a gradient of reactant concentration is established. Therefore, the entire catalyst surface is not subjected to the same concentration, thus reducing the global or effective reaction rate ($r_{m,\mathrm{eff}}$) *m* denoting that the reaction rate per unit mass of catalyst. The reaction rate when there are pore diffusion or internal mass transfer limitation, is given by $r_{m,\mathrm{int}}$ this factor is taken into consideration while determining the effective reaction rate in the upcoming sections.

$$r_{m,\mathrm{int}} = \eta\, r_m \tag{21}$$

$$\eta = \frac{\text{reaction rate with transport limitation}}{\text{reaction rate without transport limitations}} \tag{22}$$

Where η is the effectiveness factor defined by Eq. 22, r_m is the intrinsic reaction rate that depends on k_m is the rate constant and C_i is the concentrations of the gas species. The effectiveness factor ranges between 0 and 1. The pore size, catalyst shape, effective diffusivity, and reaction order directly affect the Thiele modulus used to calculate the effectiveness factor. Thiele Modulus, (ϕ) is a dimensionless number composed of the square root of the characteristic reaction rate divided by the characteristic diffusion rate in the pores. and is vital in determining pore diffusion limitations. The effectiveness factor is a function of the Thiele modulus ϕ, the effectiveness factor as a function of Thiele modulus for a flat plate shape is given by,

$$\eta = \frac{\tanh \phi}{\phi} \tag{23}$$

For a spherical particle, an effectiveness factor is given as,

$$\eta = \frac{1}{\phi}\left[\frac{1}{\tanh 3\phi} - \frac{1}{3\phi}\right] \tag{24}$$

The equation of an effectiveness factor for a flat plate can be used as a good approximation [73] for any particle geometry with a characteristic length (L_p), in Eq. 25. The Thiele modulus was developed to describe the relationship between diffusion and reaction rate in porous catalyst pellets with no mass transfer limitations

Since we are using equilibrium reactions in this work, and effectiveness factor η for a reversible reaction as a function of the equilibrium constant, the diffusion coefficient of the reactant *i*, and the characteristic length scale is determined using, Eq. 25 [20]

$$\phi = L_{\mathrm{p}} \sqrt{\left[\frac{K_{\mathrm{c}} + 1}{K_{\mathrm{c}}}\right] \frac{k_{m,i}\, \rho_{\mathrm{p}}}{D_{i,\mathrm{eff}}}} \qquad (25)$$

The characteristic length (L_{p}) is the ratio of volume of the particle to the eternal surface of the particle, it is a shape dependent parameter in the Thiele modulus, for various shapes is given by,

$$L_{\mathrm{p}} = \frac{\text{volume of shape}}{\text{external area of shape}} \qquad (26)$$

The characteristic length for the cylinder is $d_{\mathrm{p}}/4$, for a sphere is $d_{\mathrm{p}}/6$, where d_{p} is the particle diameter. Since the catalyst is of Raschig ring shape, the particle diameter is determined using the following correlation [73],

$$d_{\mathrm{p}} = \frac{3 D_{\mathrm{cat,out}}\, H_{\mathrm{cat}}}{D_{\mathrm{cat,out}} + 2\, H_{\mathrm{cat}}} \qquad (27)$$

Where $D_{\mathrm{cat,out}}$ is the outer diameter of the Raschig ring, and H_{cat} is the catalyst height. Small particles have a low characteristic length, decreasing the Thiele modulus, thus increasing the effectiveness factor and lowers the pore diffusion resistance. Furthermore, small particles size creates higher pressure drop. Therefore, it is vital to have particles with appropriate size that balance between the pressure drop across the catalyst bed and effects of diffusional resistance within the catalyst particle.

In general, inside the catalyst pellet diffusion may occur by means of molecular diffusion and Knudsen diffusion, these are called pore-volume or pore diffusion [74]. The effective diffusivity taking into consideration of two mode of internal diffusion phenomenon is given by,

$$D_{i,\mathrm{eff}} = \frac{\varepsilon_{\mathrm{p}}}{\tau_{\mathrm{p}}} D_{i,\mathrm{pore}} \qquad (28)$$

Where, ε_{p} is the porosity of the catalyst particle and τ_{p} is the tortuosity of the porous structure. Tortuosity varies with parameters such as porosity and geomentry of porous media, it is experimentally determined. It is the ratio of path lengths that a particle takes through a porous structure to the shortest length between the start and end of the same path. The value of tortuosity is always greater than or equal to 1 and porosity is typically in range of 0.25 to 0.7. The temperature and nature of diffusion has no influence on the tortuosity of the catalyst material.

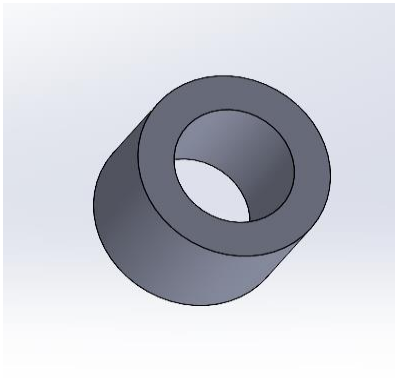

Fig. 9 Schematic of a Raschig ring shape. The Raschig ring shaped catalyst is of 5mm in diameter and 5mm in height that is compercially available.

Theoretically, in regions where the ratio of pore radius to the mean free path of the diffusing molecule is greater than 10, molecular diffusion dominates and if the ratio is less than 1, Knudsen diffusion dominates. In regions in between both diffusion phenomenon contributes to the pore mass transport and can be expressed via the Bosanquet equation [75].

$$D_{i,\mathrm{pore}} = \left[\frac{1}{D_{i,\mathrm{mol}}} + \frac{1}{D_{i,\mathrm{knu}}}\right]^{-1} \quad (29)$$

The Knudsen diffusivity of a gas species in a pore is given as,

$$D_{i,\mathrm{knu}} = \frac{d_{\mathrm{pore}}}{3}\sqrt{\frac{8\,R\,T}{\pi\,M_i}} \quad (30)$$

Where T is the temperature in Kelvin, R is the gas constant and M_i is the molecular weight of the gas species i, from Eq.30, it's evident that the Knudsen diffusion is independent of pressure and is proportional to $T^{1/2}$.

Now considering external mass transport, also known as film diffusion, the effective reaction rate due to external mass transport can be expressed as [20],

$$r_{m,\mathrm{ext}} = \beta\, A_{m,\mathrm{ext}}\left(C_{i,\mathrm{b}} - C_{i,s}\right) \quad (31)$$

Here, β is the mass transfer coefficient, $A_{m,\mathrm{ext}}$ is the external surface area of catalyst, $C_{i,\mathrm{b}}$ and $C_{i,s}$ are the concentrations in the bulk of the gas and surface of the catalyst respectively. The mass transfer coefficient β depends upon the particle size, particle geomentry, molecular diffusion coefficient, and the hydrodynamic conditions such as fluid property and velocity.

$$\beta = \frac{Sh\, D_{i,\mathrm{mol}}}{d_\mathrm{p}} \qquad (32)$$

The Sherwood number used to determine the mass transfer coefficient represents the ratio of convective to the diffusive mass transfer. Even though several correlations are used to calculate Sherwood number for a fixed bed the one proposed by Hayhurst and Parmar is used here [76],

$$Sh = [1 + 1.5(1 - \varepsilon_\mathrm{b})]\, Sh_\mathrm{p} \qquad (33)$$

Where, Sh_p is the Sherwood number for a single particle, that is calculated using the Reynolds and Schmidt number,

$$Sh_\mathrm{p} = 2 + 0.69\sqrt{Re}\sqrt[3]{Sc} \qquad (34)$$

When considering the internal and the external mass transfer limitations to calculate the global reaction rate or the effective reaction rate ($r_{m,\mathrm{eff}}$) by combining Eq. 21 and 31 we get the following expression,

$$r_{m,\mathrm{eff}} = \left[\frac{1}{r_{m,\mathrm{int}}} + \frac{1}{r_{m,\mathrm{ext}}}\right]^{-1} \qquad (35)$$

This completes the catalyst model, that gives the effective reaction rate. This reaction rate will be plugged into the molar balance in the plug flow reactor model.

3.4 Tubular reactor model

The tubular reactor model consists of conservative equations alongside with the properties of the fluid that are calculated based on the bulk temperature. The assumptions made before making the mass and energy balances are:

1. The system is at steady state (i.e., no changes with time in the system are considered) since the system is set to run continuously after starting.
2. No axial dispersion of heat or mass (i.e., plug flow, concentration and temperature are constant across the cross section), since we have low *Re* and therefore no back mixing.
3. No radial dispersion of heat or mass, since one dimension model is adequate for initial reactor design and observe the effects of process parameters.
4. The gas in the tubular reactor is ideal, valid at high operating temperature and the density of gases in the system is not high.
5. No pressure drops across the length of the reactor (i.e., at constant density). Pressure has less to no influence on the reaction since its equimolar.
6. Heating medium to the reactor is at constant temperature (i.e., wall temperature is constant throughout the length of the reactor)
7. Bed porosity is constant and the size of the catalyst particles is uniform
8. There is no heat loss, since the tube will be placed close to other tubes in the reactor and the heat lose from one tube is heat input to other tubes
9. Convection is the only mode of heat transfer in the system since heat transfer through conduction is significantly low for gases as compared to convection and there is no radiation involved in the system.
10. Catalyst is in the same temperature as the bulk phase gas temperature, since for a lab scale setup the temperature equals the gas phase temperature

3.4.1 Molar Balance

The equation we use to model the PFR at steady state is derived for taking a differential element ΔV, (Fig. 10) this volume is sufficiently small that there are no spatial variations in the reaction rate, after following the basic mass balance, we get Eq. 37 that is further mrodified for a packed bed reactor.

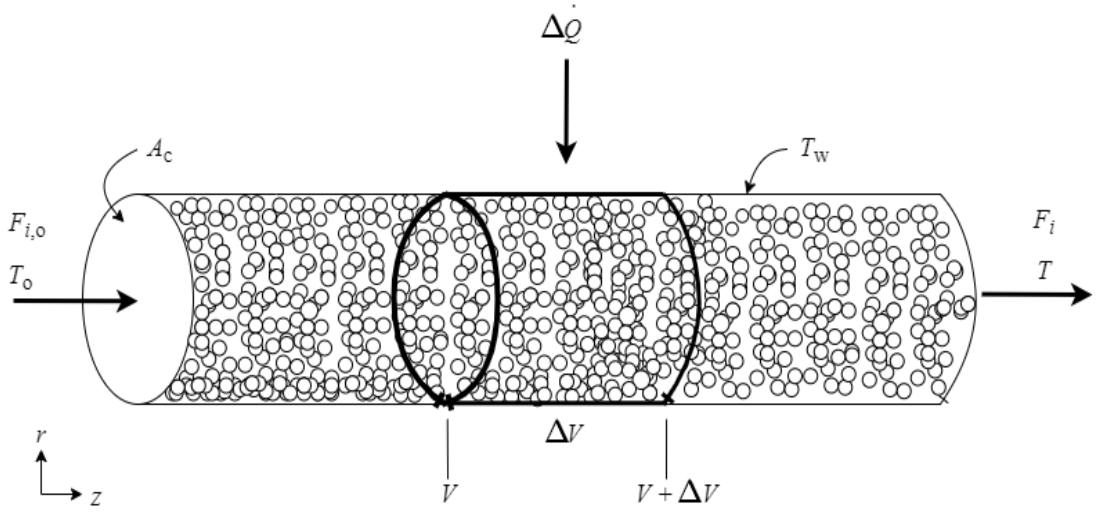

Fig. 10 Tubular packed bed reactor with catalyst particles and a constant wall heat input. A control volume ΔV is defined and this control volume is used to derive the molar and energy balance, here A_c is the crossectional area of the tubular reactor, $F_{i,o}$ and F_i are the flow rate of the component i in the reactor at inlet and outlet respectively, T_w is the wall temperature, T_o and T are the inlet and outlet temperature of the reactor respectively.

In	+	Generation	=	Out	+	Accumulation
Molar flow rate of species i into the control volume	+	Molar rate of generation of species i within ΔV	=	Molar flow rate of species i out of the control volume	+	Molar rate of accumulation of species i in the control volume
$F_{i,V}$	+	$r_i\,\Delta V$	=	$F_{i,V+\Delta V}$	+	0

Dividing by ΔV and rearranging we get,

$$\left[\frac{F_{i,V+\Delta V} - F_{i,v}}{\Delta V}\right] = r_i \qquad (36)$$

Taking the limit as ΔV approaches zero, we obtain the differential form of steady state mole balance on a PFR.

$$\frac{\mathrm{d}F_i}{\mathrm{d}V} = r_i \tag{37}$$

The derivation of the design equation for a packed bed reactor (PBR) will be carried out in a manner analogous to the development of the tubular reactor design equation, this is done by replacing the volume coordinate in Eq. 37 with the catalyst mass coordinate *W*. Also, the reaction rate is for per unit mass of catalyst.

$$U_\mathrm{s}\frac{\mathrm{d}C_i}{\mathrm{d}z} = \rho_\mathrm{b}\, r_{m,i} \tag{38}$$

This molar balance gives us the composition of component *i* with respect to increasing total mass of the catalyst in the reactor. This can be further contemplated to give the compositions of the components in the reactor along the length of the reactor.

3.4.2 Energy Balance

The energy balance over the same differential element ΔV is used to calculate the axial temperature profile inside the reactor. From the assumption stated above the energy equation is given as,

In	+	Generation	=	Out	+	Accumulation
Rate of energy added into the system by mass flow in	+	Rate of flow of heat to the system from the surrounding	=	Rate of energy leaving the system by mass flow out	+	Rate of work done by the system on the surrounding
$\sum F_\mathrm{in}E_\mathrm{in}$	+	$\dot{Q}$	=	$\sum F_\mathrm{out}E_\mathrm{out}$	+	$\dot{W}$

Where *E* is the sum of the internal energy (*U*), the kinetic energy, the potential energy, and others such as electric or magnetic or light energy, in most chemical reactor situation, the kinetic, potential, and other energies are negligible in comparison with the enthalpy the above equation becomes,

$$\dot{Q} + \sum F_{i,\mathrm{in}}H_{i,\mathrm{in}} - \sum F_{i,\mathrm{out}}H_{i,\mathrm{out}} = 0 \tag{39}$$

Were $\dot{Q}$ is the heat flow to the reactor,

$$\dot{Q} \;=\; U\,\Delta A\,(T_{\mathrm{w}} \;-\; T) \;=\; U\;a\;\Delta V\;(T_{w} \;-\; T) \qquad (40)$$

Where a is the heat exchanging area per unit volume of the reactor. For a tubular reactor,

$$a \;=\; \frac{A}{V} \;=\; \frac{\pi\,D\,L}{\frac{\pi\,D^{2}L}{4}} \;=\; \frac{4}{D} \qquad (41)$$

Substituting for $\dot{Q}$ in Eq. 39 and dividing by ΔV and then taking limit of ΔV to zero, we get

$$U\;a\;\Delta V\;(T_{\mathrm{w}} - T) - \sum \frac{\mathrm{d}F_{i}}{\mathrm{d}V} H_{i} \;- \sum \frac{\mathrm{d}H_{i}}{\mathrm{d}V} F_{i} \;=\; 0$$

From the molar balance we get,

$$\frac{\mathrm{d}F_{i}}{\mathrm{d}V} = r_{i} = v_{\mathrm{i}}(r_{\mathrm{a}})$$

where, v_{i} is the stoichiometric coefficient and r_{a} is the reaction rate in terms of species a. Using the thermodynamic expression of enthalpy and substituting the enthalpy of reaction into the below equation we get Eq. 42 as the energy equation for a plug flow reactor,

$$Ua(T_{\mathrm{w}} - T) - \sum v_{\mathrm{i}}\,H_{\mathrm{i}}\underbrace{(r_{\mathrm{a}})}_{\Delta H_{\mathrm{rxn}}} - \sum F_{\mathrm{i}}\,C_{p}\frac{\mathrm{d}T}{\mathrm{d}V} \;=\; 0$$

Rearranging the terms for the temperature, we get

$$\frac{\mathrm{d}T}{\mathrm{d}V} \;=\; \frac{(r_{\mathrm{i}})\Delta H_{\mathrm{rxn}} - \;Ua\;(T - \;T_{\mathrm{w}})}{\sum F_{\mathrm{i}}\,C_{p_{i}}} \qquad (42)$$

Since we are using a packed bed reactor setup, we again replace the volume coordinate with the weight coordinate W, i.e. ($\mathrm{d}W = \rho_{\mathrm{b}}\,\mathrm{d}V$). Also, the reaction rate is for per unit mass of catalyst ($r_{m,i}$), therefore,

$$\frac{\mathrm{d}T}{\mathrm{d}W} \;=\; \frac{(\,r'_{i})\Delta H_{\mathrm{rxn}} - \;\dfrac{Ua\;(T - \;T_{\mathrm{w}})}{\rho_{\mathrm{b}}}}{\sum F_{i}\,C_{p_{i}}} \qquad (43)$$

Writing the equation along the length of the reactor,

$$\frac{\mathrm{d}T}{\mathrm{d}z} = \frac{\frac{(r'_i)\,\Delta H_{\mathrm{rxn}}}{\rho_{\mathrm{b}}} - Ua\,(T - T_{\mathrm{w}})}{\sum F_i\, C_{p_i}} A_{\mathrm{c}} \qquad (44)$$

This completes the energy balance for the PBR, to determine the temperature profile along the axis of the reactor.

3.4.3 Pressure drop

In addition to temperature and concentration distributions in the packed bed, the pressure drops over the reactor is an important reactor characteristic. The pressure drop is rarely than 10% of the total pressure [69]. Considering inaccuracies in the reaction rate expressions and the uncertainties in the transport parameters, the pressure drop does not usually have a significant effect on the overall model performance. The effect of pressure drop on transport properties such as viscosity, thermal conductivity, and specific heat capacity, for a 1 bar pressure drop across the reactor length was 0.002% different compared to the inlet conditions (Appendix A.1.3). Also, pressure has less effects on the reactor model since reverse water gas shift has equimolar reactant and products. Nevertheless, pressure drop might be of great importance for assessment of the reactor operation costs. Therefore, pressure drop is studied separately using the most often used Ergun equation for flow through a packed column [79],

$$\frac{\mathrm{d}p}{\mathrm{d}z} = \frac{\rho_f u_{\mathrm{s}}^2}{2} \frac{1}{d_p}\, 4\, f \qquad (45)$$

Where, ρ_f is the fluid density, u_{s} is the superficial gas velocity, d_p is the equivalent particle diameter, f is the friction factor calculated using empirical relation from [80],

$$f = \frac{(1 - \varepsilon_{\mathrm{b}})}{2\,\varepsilon_{\mathrm{b}}^3} \left[\frac{\alpha\,(1 - \varepsilon_{\mathrm{b}})}{Re} + \beta\right] \qquad (46)$$

Where, α = 150, β = 1.75, and ε_{b} is the porosity of the bed.

3.4.4 Overall model summary

The base model consists of the catalyst and the tubular reactor model combined, it first constitutes for the RWGS reaction with molar balances for each species and the overall energy balance of the reactor. The set of differential equations are solving using the initial value of the concentration that are the inlet conditions of the reactor.

$$a\ CO_2 + b\ H_2 \leftharpoons c\ CO + d\ H_2O \quad (47)$$

The kinetics of the reactions based on the previous works done by Unde. R.B et al [28]. The global reaction rate calculated using the catalyst model is the plugged in the reactor model to calculate the concentration along the length of the reactor. For the RWGS reaction the effective or the global reaction rate after incorporating the mass transfer limitations are given by Eq. 48.

$$r'_{\mathrm{eff},CO_2} = \left[\frac{1}{\eta_{CO_2}\, k_{m,CO_2} C_{CO_2}^{0.1} C_{H_2}^{0.4}} + \frac{1}{\beta A_{m,\mathrm{ext}}\left(C_{CO_2} - C_{CO_2,\mathrm{eq}}\right)}\right]^{-1} \quad (48)$$

The effective reaction rate is calculated based on two assumptions by Unde. R.B et al, firstly, the reverse reaction was not considered in the pore diffusion term, because the influence of the reverse reaction is less compared to the forward reaction at operating conditions. Secondly, for the external mass transfer, the equilibrium concentration is assumed at the external surface for simplicity of the model. Since the concentration at the surface of the catalyst is very difficult to measure and validate for a porous catalyst. This value is higher and only reached if the chemical reaction is very fast.

The reaction rates are coupled by using relative rates of reaction, i.e using the stoichiometric relationship between reacting molecules for a single reaction. The rates of species formation or disappearance for RWGS mentioned above is given as,

$$\frac{r'_{\mathrm{eff},CO_2}}{-a} = \frac{r'_{\mathrm{eff},H_2}}{-b} = \frac{r'_{\mathrm{eff},CO}}{c} = \frac{r'_{\mathrm{eff},H_2O}}{d} \quad (49)$$

Where *a*, *b*, *c*, *d* are stoichiometric coefficients of each species in the reaction, since the rate of disappearance of CO_2 is known, we can find the other species rates of formation or disappearance. Similarly, for the methanation reaction (Eq.50), we know the rate of disappearance of CO as given by Eq.51, therefore the rates of other species can be determined.

$$CO + 3H_2 \leftharpoons CH_4 + H_2O \quad (50)$$

$$r'_{\text{eff,CO}} = \left[\frac{1}{\eta_{\text{CO}}\, k_{m,\text{CO}} C_{\text{CO}}^{-0.3} C_{\text{H}_2O}^{0.7}} + \frac{1}{\beta\, A_{m,\text{ext}}\left(C_{\text{CO}} - C_{\text{CO,eq}}\right)}\right]^{-1} \quad (51)$$

Now the overall system of differential equation that gives the rate of production or disappearance of each species with respect to the length of the reactor is given as,

$$U_s \frac{dC_{CO_2}}{dz} = \rho_b * -r'_{eff,CO_2,\ RWGS} \quad (52)$$

$$U_s \frac{dC_{H_2}}{dz} = \rho_b \left(-r'_{eff,H_2,\ RWGS} - 3 * r'_{eff,H_2,\ Methantion}\right) \quad (53)$$

$$U_s \frac{dC_{CO}}{dz} = \rho_b \left(r'_{eff,CO\ RWGS} - r'_{eff,CO\ Methanation}\right) \quad (54)$$

$$U_s \frac{dC_{H_2O}}{dz} = \rho_b \left(r'_{eff,H_2O\ RWGS} + r'_{eff,H_2O\ Methanation}\right) \quad (55)$$

$$U_s \frac{dC_{CH_4}}{dz} = \rho_b * r'_{eff,CH_4,\ Methanation} \quad (56)$$

The energy balance for the axial temperature profile of the reactor with both methanation and the RWGS reaction.

$$\frac{\mathrm{d}T}{\mathrm{d}z} = \frac{\frac{\sum_{i=1}^{n}\left(r'_{ij}\right)\Delta H_{\text{rxn},ij}}{\rho_{\text{b}}} - Ua\,(T - T_{\text{w}})}{\sum_{j=1}^{m} F_j C_{p_j}} A_{\text{c}} \quad (57)$$

Where, *i* is the reaction number and *j* are the species in the reaction. The Equation from 52 to 57 completes the set of ordinary differential equations that will be solved in python using the ODEint function. The inlet concentrations of each species, and the inlet conditions are used to solve the ODE.

4 Results and Discussion |

The model detailed in chapter 3 was implemented in python, the step involved in the implementation of the model is discussed briefly in the preliminary stages of this chapter, and later simulation results from the implemented model are presented. At the end of this chapter, the results are analyzed and discussed to estimate the optimal operating conditions for the reverse water gas shift reactor.

4.1 Model Implementation

The RWGS reaction was first modeled, without the mass transfer limitations incorporating the reaction kinetics from Unde et.al [28]. The initial modeling parameters used to create the base model with RWGS reaction are listed below in Table 3 The molar balance was initiated successfully for an isothermal condition the resulting composition is compared with the equilibrium calculations at the same temperature and pressure, before including the energy balance.

Table 3 : Input data and reactor conditions used to model a plug flow tubular fixed bed reactor.

Pressure, P	20 bar
Tube length, L	6 m
Tube outer diameter, d_o	60.3 mm
Tube wall thickness	2.77 mm
Space velocity	3000 Nm^3 gas / m^3 catalyst
Inlet temperature, T_i	650^oC
Bulk density of catalyst, ρ_b	950 kg/m^3
Porosity	0.48
Wall temperature, T_w	950^oC

Before including the energy balance, the fluid properties such as viscosity, thermal conductivity, specific heat capacity, and enthalpy of reaction are determined for varying temperature profile along the length of the reactor [Appendix A2]. Both energy balance and molar balance are coupled via the reaction rate, the coupled ordinary differential equations are solved using the *odeint* function in python. The inital conditions used to solve the ODE are the inlet composition of all components in the system and inlet temperature of the feed, additional a constant wall temperature is used as boundary condition at the reactor wall. The above mentioned is the base model, with the reaction rate that is not mass transfer limited, the mass transfer limitations are incorporated into

the base model using the catalyst model and the plug flow tubular reactor model is completed. In Fig. 11, shows the composition along the reactor length for an equimolar feed composition of CO_2 and H_2 with 60.1% conversion of CO_2 at the end of the reactor length.

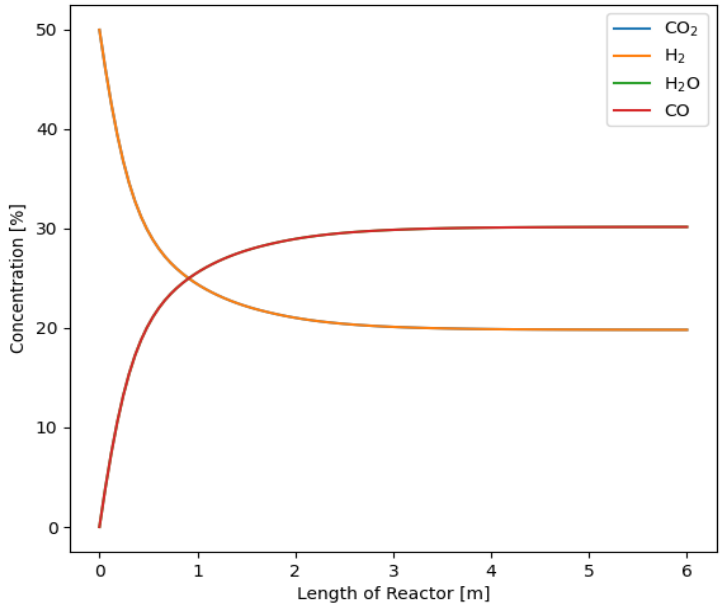

Fig. 11 (a) Concentration profile of CO_2, H_2, CO, and H_2O along the length of the tubular RWGS reactor with T_{inlet} = 650°C, T_w = 950°C, and equimolar inlet composition H_2:CO_2 [1].

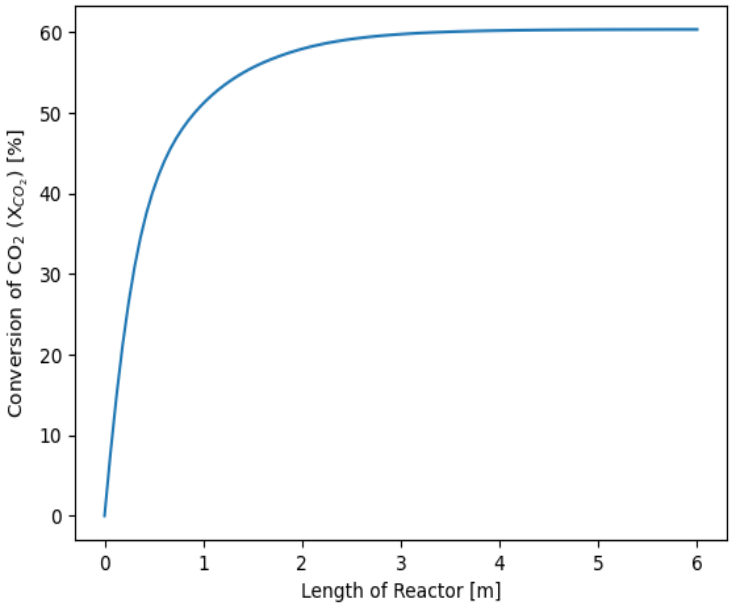

Fig. 11 (b) Conversion of CO_2 along the length of the tubular RWGS reactor T_{inlet} = 650°C, T_w = 950°C, and equimolar H_2:CO_2 at inlet with 60.1% conversion of CO_2 at 6 meters

Later, the methanation reaction (CO Hydrogenation) kinetics as per chapter 3 were included in the base RWGS tubular reactor model to complete the model. Similar to the

[1] The concentration of CO and H_2O overlaps each other in the figure and similarly CO_2 and H_2 overlaps because of equimolar inlet composition of CO_2 and H_2

RWGS reactor model, the effective reaction rate is determined by the catalyst model over a Nickel on Calcium Aluminate catalyst. The determined effective reaction rate of CO hydrogenation is incorporated in the molar balance to determine the concentration of each species (CO_2, H_2, CO, H_2O, and CH_4) along the length of the reactor.

The output from the model is the concentrations and axial temperature profile. The primary derivation from the concentration and temperature profile is to identify the heat input and the space velocity required to achieve the desired conversion at the outlet. Therefore the composition at the reactor exit is useful for downstream FT synthesis. The secondary derivation is operating window for the functioning of the reactor without carbon formation. As discussed in chapter 2, boudouard reaction or CO disproportionation (Eq.7) leads to carbon formation. To quantify the operating region that is susceptible to carbon formation, carbon activity for the boudouard reaction is calculated. Activity is an effective concentration, based on the chemical potential.

$$2\mathrm{CO(g)} \leftrightharpoons \mathrm{C(s)} + \mathrm{CO_2(g)} \qquad \Delta_r H^o = -172.4\ \mathrm{kJ/mol} \tag{7}$$

The equilibrium constant for boudouard is given by,

$$\mathrm{K_{eq,actual}} = \frac{p_{\mathrm{CO_2}}}{p_{\mathrm{CO}}^2} \tag{58}$$

Where, p_{CO} and $p_{\mathrm{CO_2}}$ are the partial pressures of CO_2 and CO respectively. Similarly, equilibrium constant for carbon formation on Ni based catalyst is given by Eq.59,

$$\begin{aligned}\mathrm{K_{eq,Ni}} = \exp(&60.4 - 0.499\,T + 1.92\,.\,10^{-3}\,T^2 - 3.65\,.\,10^{-6}\,T^3 \\ &+ 3.59\,.\,10^{-9}\,T^4 - 1.77\,.\,10^{-12}\,T^5 + 0.35\,.\,10^{-15}\,T^6\,)\end{aligned} \tag{59}$$

This equation is an empirical result that predicts the equilibrium well. $K_{eq,Ni}$ increases with raise in temperature therefore signifying boudouard is favored at low temperature. The direction of boudouard is predicted by dividing $K_{eq,Ni}$ by $K_{eq,actual}$. If the ratio calculated is less than 1, then the equilibrium is shifted towards CO_2 production so any solid carbon will be converted to CO, therefore no net formation of carbon. If carbon activity greater than 1 then equilibrium shifts to the right and CO is converted to CO_2 and carbon

4.2 Model Validation

The model is validated by making the reactor length longer than 6 meters to achieve unfluctuating values in the concentration of components in the system. Since there are no changes in the composition of the reactant and products, the system is assumed to be in equilibrium. Concentration or partial pressure are used to calculate the equilibrium constant. On the other hand, equilibrium constant is calculated based on temperature, the expression for equilibrium constant K_p as a function of temperature for RWGS reaction is given by Twigg [55],

$$K_{\text{p (actual)}} = \frac{1}{\exp\left(-0.29353Z^3 + 0.63508\,Z^2 + 4.1778\,Z + 0.31688\right)}$$

Were, $Z = \left(\frac{1000}{T(K)}\right) - 1$

Since the model is at equilibrium the $K_{\text{p (actual)}}$ and the $K_{\text{p (model)}}$ must be identical or in close proximity to know that the model is producing reasonable results.

The concentration or partial pressure for an equimolar inlet composition of H_2 and CO_2 condition is obtained to test the model. The reaction rate used for modelling the tubular reactor takes into consideration only the forward reaction of a reversible reaction. The same is used despite neglecting the reverse reaction because water-gas-shift (reverse reaction) is not favorable in higher temperatures. In our case the reactor is operating above 650^{o}C, that favours RWGS. The model is used to evaluate the carbon formation and methane formation for a very specific catalyst (Nickel on Calcium Aluminate). Due to Ni based catalyst are the focus of interest on future experimentations and kinetics for other Ni based catlaysts for RWGS were not widely available in literatures. Using the reaction rate mentioned in (Eq.48) the partial pressure at the outlet are determined and the equilibrium constant is determine.

The partial pressures determined by the model is then used to calculate the equilibrium constant using the following,

$$K_{\text{p (model)}} = \left(\frac{p_{CO}\,p_{H_2O}}{p_{CO_2}\,p_{H_2}}\right) \qquad (60)$$

An overestimation of products CO and H_2O in the outlet is determined apon comparing the K_p from model and actual. The actual equilibrium constant calculated using temperature according to Twigg [55] at 1223K is lower compared to the equilibrium constant determined via the model estimated an equilibrium constant. High equilibrium constant signifies forward reaction is favoured, also the conversion of CO_2 exceeded the equilibrium conversion of CO_2 for an equimolar inlet composition.

These explains the overestimation of CO is due to kinetics. To determine the effect of not incorporating the water-gas-shift reaction and to quantify the significane in overestimation, an elementary reaction rate is introduced to determine the equilibrium constant via the model. Later, the partial pressures from the model is compared with the

results obtained from not including the reverse reaction rate to assess the difference in results. Therefore implication of not including the reverse reaction is quantified and limitations for the model can be determined.

The reaction rate for consumption of CO_2 is given by Eq.61 [28] incorperating the reverse reaction assuming RWGS as an elementary reaction (i.e. all the exponents in the concentration terms of reactants and products are 1). This reaction rate (Eq.61) is used to calculate the effective reaction rate incorporating the internal and external mass transfer limitations via catalyst model and later the partial pressures are found and tabulated (Table 4).

$$r'_{CO_2} = k_{m,CO_2}\left[C_{CO_2} - \frac{C_{CO}\, C_{H_2O}}{K_p\, C_{H_2}}\right] \quad (61)$$

For an equimolar feed composition of H_2:CO_2 = 1; the following partial pressures are obtained from the model,

Table 4 : Partial pressures of reactant and products at the outlet of the reactor with length 10 meters and inlet composition of H_2:CO_2=1 and 1223K outlet temperature.

p_{CO_2}	4.474 bar
p_{H_2}	4.474 bar
p_{CO}	5.525 bar
p_{H_2O}	5.525 bar

These partial pressures of reactant and product are evaluated at the outlet of the reactor with length 10 meters. The temperature at the outlet of the reactor is 1223K, the equilibrium constant at the reactor outlet temperature is calculated using the $K_{p\,(actual)}$. The results are compared in table below,

Table 5 : Comparison of equilibrium constants calculated based on temperature using equation denoted by $K_{p\,(actual)}$ *and* $K_{p\,(model)}$ *calculated using equation 60. The last column is the difference in the equillbrium constants calculated by both the methods.*

$K_{p\,(actual)}$	$K_{p\,(model)}$	ΔK_p
1.5250080073557761	1.5250080073579617	$2.185 \cdot 10^{-12}$

The error between the equilibrium constant of actual and model is in the range of 10^{-12}, therefore it is taken to be negligible, therfore the catalyst and the tubular RWGS reactor model is producing significant results. It is determined that by neglecting the reverse reaction, the composition of CO and H_2O are overestimated by 1.57032% more than the equilibrium's volume composition at the reactor outlet. Therefore the reaction rate is slightly fast when the reverse reaction is not incorporated, but the difference are marginal.

In perspective of carbon formation overestimation of CO is better, since higher partial pressure of CO results in more susceptibility for formation of carbon in the reactor. On the other hand, methantion formation also increases as overestimation of CO, since CO and H_2 will be largely available in the reactor. Implying, methanation and carbon formation are investigated at conditions that are more favorable. Ensuring a buffer between the model and realistic cases.

4.3 Modelling results

The system was setup to determine the concentration and the axial temperature profile along the length of the reactor; the operating parameters such as the inlet composition, inlet gas temperature, fixed wall temperature, are varied to see their effect on the concentration along the length of the reactor and consequently the amount of carbon and methane formation in the tubular reactor model.

4.3.1 Inlet composition

The produced syngas via the RWGS reactor is downstream used for the Fischer Tropsch synthesis. The appropriate syngas composition for operating the Fischer – Tropsch reactor is between 1.8 to 2.1. From thermodynamic equilibrium analysis it was observed that having different composition of H_2 and CO_2 in the system produced significant changes in the equilibrium composition at varying temperatures. Thus, H_2:CO_2 ratio at the inlet was varied from 1 - 4 to obtain the composition of reactants and products along the length of the reactor. This identifies the appropriate GHSV that determines the length of the reactor and the feed composition for downstream FT synthesis with effective use of the catalyst. The inlet composition of reaction gas mixture consists here are of only CO_2 and H_2, other operating conditions used for modelling are as following in Table 3. For an equimolar to higher H_2:CO_2 ratios the conversion of CO_2 increases with increase in H_2:CO_2 ratio as show in Fig.12. Additionally at higher ratios of H_2:CO_2, CO_2 is the limiting reactant therefore no more conversion is observed beyond limited reactor lengths resulting in flat line after 0.75 meters at H_2:CO_2 ratio of 3 in Fig 12. The reaction rate of RWGS depends on concentration of H_2 as compared to CO_2 therefore the reaction rate is quicker for higher ratios of H_2:CO_2. Desired syngas composition are never achieved for ratio > 2, with 950 deg wall temperature. Even the conversion is low required composition and temperature are attained at lower H_2:CO_2 ratios.

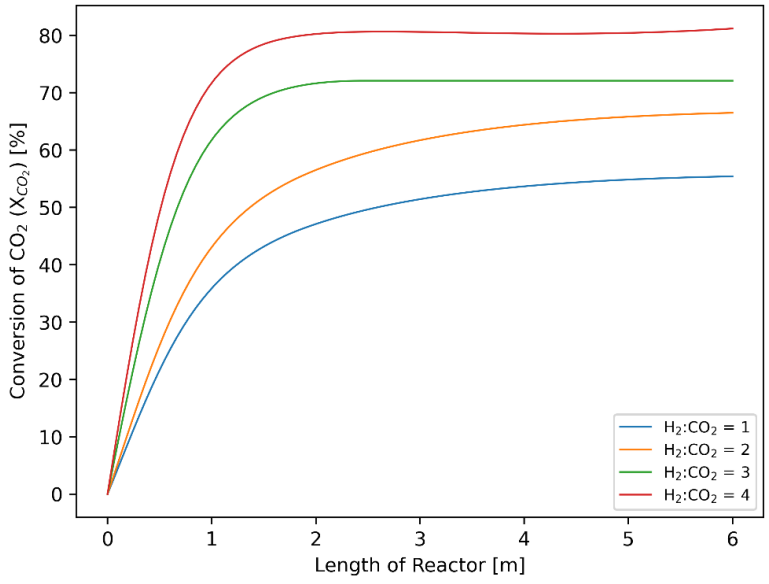

Fig. 12 Conversion of CO_2 (X_{CO_2}) for varying inlet composition of H_2:CO_2 along the length of the tubular RWGS reactor with T_{inlet} = 650°C, T_w = 950°C, and 20 bar.

For an equimolar inlet feed composition (Fig. 13), the concentration of CO_2 and H_2 decreases along the length of the reactor since the temperature increases and CO_2 is converted to CO and H_2O alongside the formation of methane at the end of the reactor due to availability of H_2 and the CO produced from RWGS, the amount of methane produced is verified with the equilibrium composition of methane at 950^{o}C and H_2:CO_2 = 1. The methane composition is as expected at ~ 3.8% of the composition of gas at the reactor outlet for the given gas hourly space velocity (GHSV) of 3000 Nm^3 gas / m^3 catalyst for H_2:CO_2 =1.

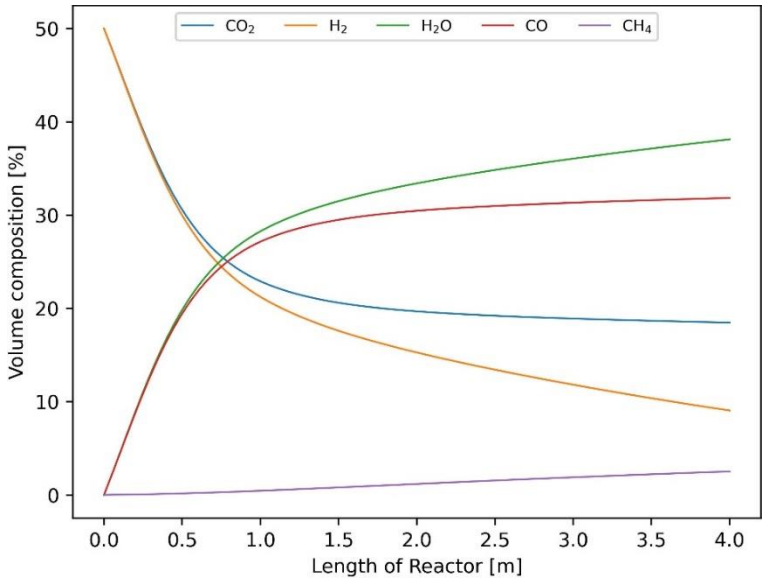

Fig. 13 Concentration profile of reactants and products along the length for equimolar feed composition of H_2:CO_2 with T_{inlet} = 650^{o}C, T_w = 950^{o}C, GHSV = 3000 h^{-1} and 20 bar pressure

The methanation reaction predominantly occurs after the RWGS produces CO, the carbon monoxide is then converted to methane via the CO hydrogenation. The effects of feed composition on the methane formation are performed by analyzing the concentration profiles for different H_2:CO_2 ratio above 1. As the concentration of H_2 increased from equimolar to 4 times the concentration of CO_2 in the inlet, the production of methane increased from 4.5% to 14.2% volume percentage respectively of the total composition of the outlet gas stream. This is due to the higher availability of H_2 and CO at higher ratio of H_2:CO_2 as compared to the equimolar inlet composition. For varying the inlet composition, the volume percentage of each component along the reactor are shown in Fig 14. As the H_2:CO_2 ratio increased the volume percentage of H_2O along the length of the reactor also increases, because H_2O being the product of both RWGS and methanation.For H_2:CO_2 ratio greater than 2, significant part of the reactor produces methane and not reaching higher conversion of CO_2. Since RWGS reaching equilibrium the availability of unreacted H_2 drive the methane formation. This impacts the H_2:CO ratio of syngas since H_2 decrases significantly compared to CO. A similar observation was made during the thermodynamic equilibrium analysis where composition of methane was high for higher H_2:CO_2 at similar operating temperature.

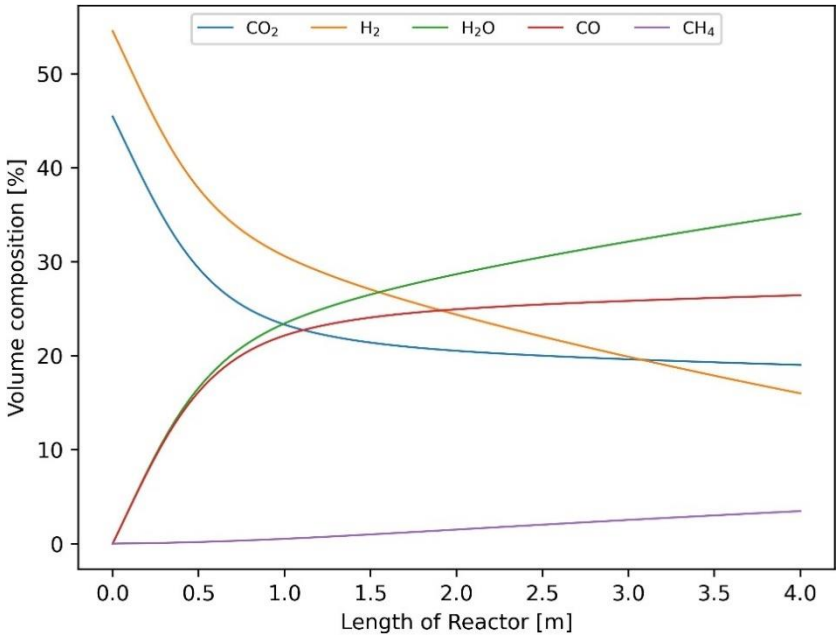
CO2
H2
H2O
CO
CH4
Volume composition [%]
Length of Reactor [m]
0
10
20
30
40
50
0.0
0.5
1.0
1.5
2.0
2.5
3.0
3.5
4.0

(a)

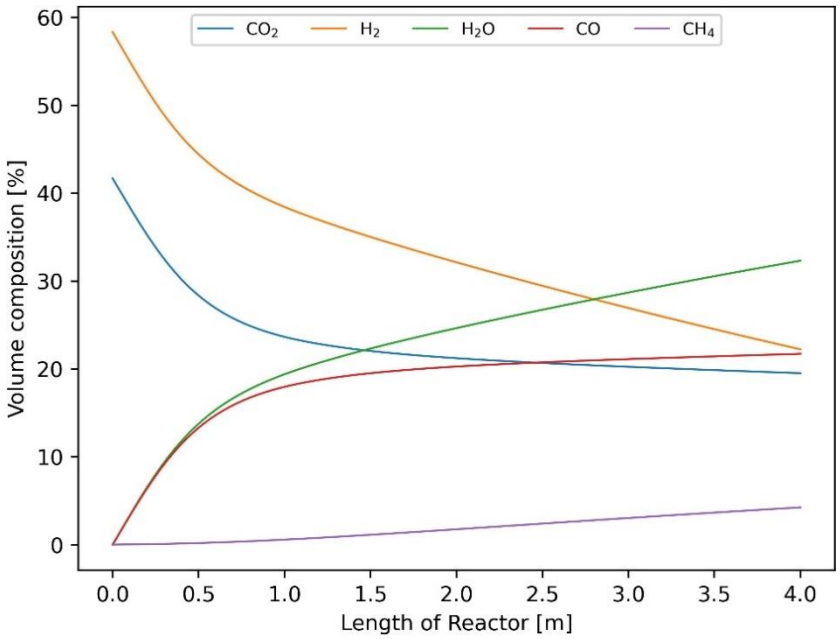
CO2
H2
H2O
CO
CH4
Volume composition [%]
Length of Reactor [m]
0
10
20
30
40
50
60
0.0
0.5
1.0
1.5
2.0
2.5
3.0
3.5
4.0

(b)

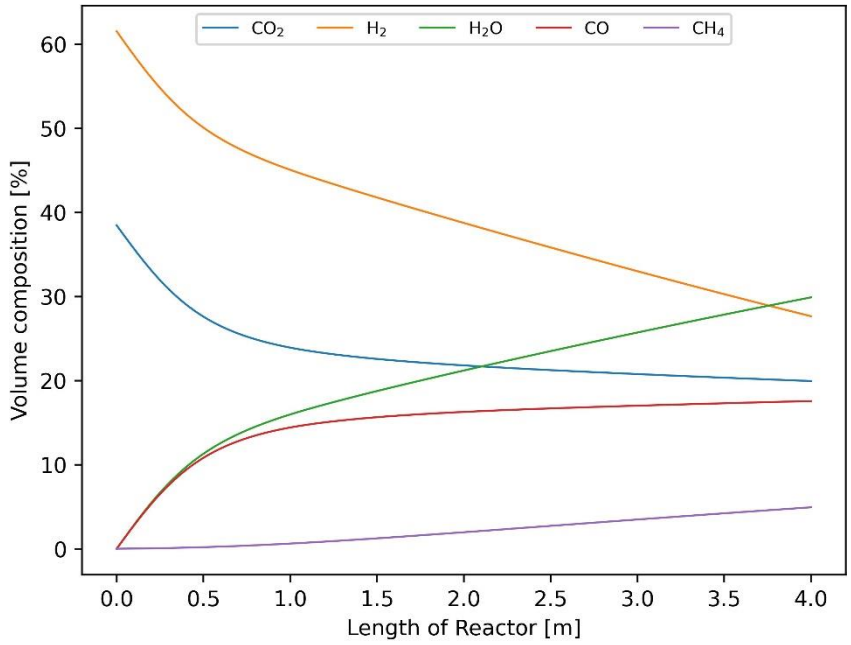

(c)

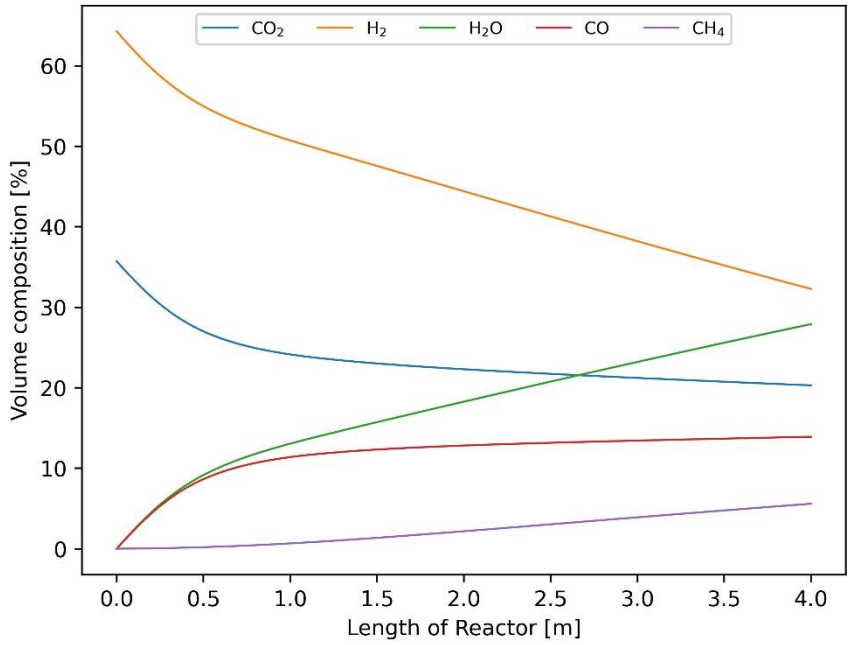

(d)

Fig. 14 Concentration profile of reactants and products along the length of the reactor for (a) H_2:CO_2 =1.2 ; (b) H_2:CO_2 =1.4 ; (c) H_2:CO_2 =1.6 ; (d) H_2:CO_2 =1.8 with T_{inlet} = 650°C, T_w = 950°C, GHSV = 3000h^{-1} and 20 bar pressure.

Furthermore, for H_2:CO_2 ratios greater than 2, the composition of H_2 is always more than twice of CO because RWGS is an equimolar reaction and CO_2 is the limiting reactant at higher ratios of H_2:CO_2. At H_2:CO_2 = 3 the outlet composition of H_2 is 3.2 times that of CO (Fig.15), similarly for H_2:CO_2 = 4 the outlet composition of H_2 is 4.46 times that of CO. For ratios of H_2:CO_2 < 2, CO does not decrease with increase in methane concentration. The rate of formation of CO via RWGS is higher than rate of consumption of CO via the methanation reaction for H_2:CO_2 < 2. The concentration of CO increases quickly and is followed by small increments due to the net reaction rate of CO close to equilibrium. Additionally, conversion of CO_2 and CO produces H_2O in the outlet stream as a major byproduct, it consists of 30.1% and 27.2% for H_2:CO_2 = 3 and H_2:CO_2 = 4 respectively at the reactor outlet. Therefore, the partial pressure of H_2O is always the high for all inlet compositions implying potential for carbon formation at the exit of the reactor is low. The concentration profiles of components in the reactor for lower concentration profiles between 1 – 2 with an increasement of 0.2 from H_2:CO_2 is shown in Fig.14.

From the above-mentioned graphs it is known at certain lengths of the reactor, desired outlet composion (i.e, H_2:CO ratio) and temperature are satisfied. Initially the reactor length was kept at 4 meters with space velocity of 3000 h^{-1}. It is observed the kinetics at the start of the reactor length is fast signifying the higher conversion of CO_2 and H_2 and beyond 1.5 meters the composition are very close to equilibrium. The reactor after 2 meters does not increase the conversion of CO_2 but aids in production of methane. From the model it is evident to take advantage of the fast kinetics at the initial length of the reactor. Therefore, higher space velocity is used to get the most out of the catalyst volume in the reactor. Higher GHSV results in shorter reactor length. It is convenient to use GHSV as an input parameter in the future to determine the optimal length and subsequently the catalyst volume for design considerations. Since the composition reaches very close to the equilibrium at length 1.5 meters, but the desired composition of syngas is different that desired. Inlet and wall temperature is then utilized to obtain the desired outlet compositions of the reactor.

The GHSV is increased in steps of 1000 h^{-1} for an inlet temperature of 650^{o}C and wall temperature of 950^{o}C the model resulted in similar conversion of CO_2 till 6000 h^{-1}. For GHSV greater than 6000 h^{-1} the conversion was less compared to that obtained for GHSV of 3000 h^{-1} at given inlet and wall temperature respectively. At 6000 h^{-1} the outlet temperature was in the desired range above 850^{o}C, but the composition of syngas (H_2:CO) was greater than 2.1. The desired syngas composition for downstream FT synthesis is between 1.8 to 2. When the inlet temperature is increased from 650^{o}C to 750^{o}C, the outlet composition of syngas (H_2:CO) decreases from 2.2021 to 2.0015. A similar effect on outlet composition is observed when keeping the inlet temperature at 650^{o}C and increasing the wall temperature from 950^{o}C to 975^{o}C. The syngas composition decreased from 2.2021 to 1.996867 satisfying the required composition for downstream FT synthesis. The outlet temperature and the syngas composition are satisfied for both cases therefore the length of the reactor is determined to be 2 meter with an GHSV of 6000h^{-1}

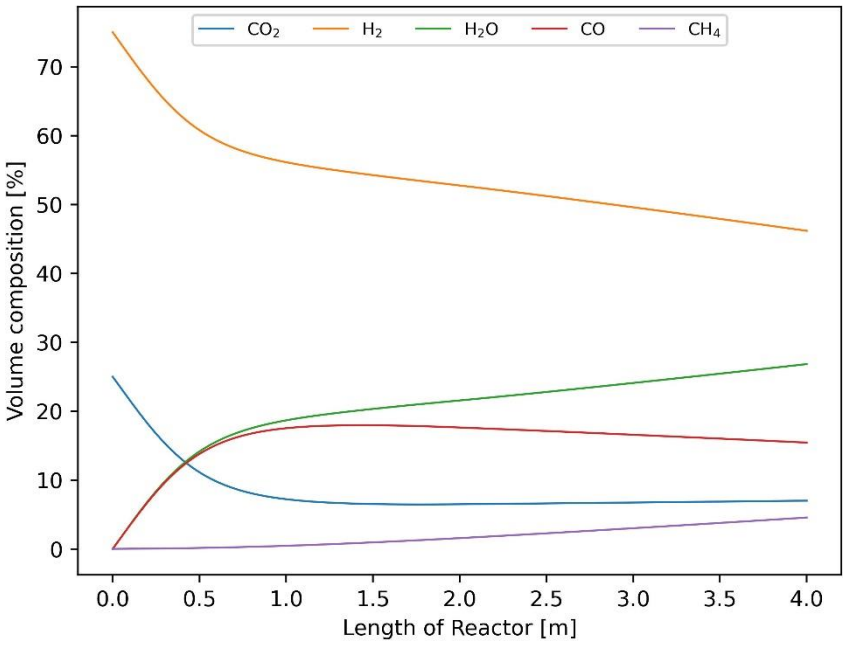

Fig. 15 Concentration profile of reactants and products along the length of the reactor for higher H_2:CO_2 ratio of 3 with T_{inlet} = 650°C, T_w = 950°C, GHSV = 3000 h^{-1} and 20 bar pressure. The CH_4 is high due to conversion of CO to CH_4 and 8% of CH_4 found at length 4 meter.

The carbon formation is evaluated as discussed in section 4.1; operating conditions are to be established in such a way that; no carbon formation occurs along the length of the reactor. Not only because it deactivates the catalyst and reduces reaction rate by blocking the pores of catalyst etc., but mainly due increased pressure drop due to blocked area, as well as corrosion issues due to carburization of the metal surfaces in the reactor. This cause shutdown of the reactor for loading fresh catalysts that cause less production. The reduction operational costs can be significantly reduced if carbon formation is completely avoided. Since RWGS tubular reactor is the first step in producing raw material for the downstream FT-synthesis to produce hydrocarbons. A qualitative approach is followed in identifying if carbon formation is favored in the system or not. Since boudouard reaction is a reversible reaction, the method to predict the direction in which the equilibrium shifts is used to qualify if carbon formation occurs at given composition and operating conditions.

The equilibrium constant is evaluated as a function of temperature, the operating temperature across the length of the reactor is obtained from the model, this gives the Equilibrium constant (K_{eq}). From the concentration profiles, the reaction quotient Q for the boudouard reaction is calculated using Eq.58, the reaction quotient is the ratio of product to reaction concentration when not in equilibrium. Using Q and K_{eq} the direction in which the reaction is favored can be identified.

There are three possible cases as listed below in table 6,

Table 6 : Three cases for a reversible reaction to determine the way in which the reaction proceed based on the equilibrium constant K_{eq} and reaction quotient Q.

Case 1	$Q = K_{eq}$	The reaction is in equilibrium
Case 2	$Q > K_{eq}$	The reverse reaction is favored, reaction moves from right to left
Case 3	$Q < K_{eq}$	The forward reaction is favored, reaction moves from left to right

For simplification case 2 is chose since it can be used to written case 3 using inequalities.

- If, $K_{eq}\ dividied\ by\ Q\ is\ less\ than\ 1$; then net carbon formation is zero, i.e., the produced carbon reacts with CO_2 in the reactor and forms CO. The risk of carbon formation in the reactor is thus minimal.

- If, $K_{eq}\ dividied\ by\ \ Q\ is\ greater\ than\ 1$; then net carbon formation is not zero, i.e., the CO in the reactor system is favored to be converted to carbon and CO_2 at given operating conditions.

Both these conditions are for the boudouard reaction written as,

$$2CO(g) \leftharpoons C(s) + CO_2(g)$$

Therefore using Eq. 58 and 59, the equilibrium constant and the equilibrium quotient are determined to evaluate the potential of carbon formation called the carbon activity. This carbon activity is a dimensionless number , that is plotted against the length of the reactor to determine where and at what operating conditions carbon activity is more than 1 thus leading to carbon formation in the reactor.

Using the concentrations from the model, the concentration are proceeded to predict the carbon activity using the method mentioned above. The carbon activity for ratios of H_2:CO_2 that produced the required syngas composition are evaluated and plotted along the length of the reactor (Fig 16). For an equimolar inlet ratio of H_2 and CO_2 the carbon activity increases rapidly at the inlet of the reactor till 0.5 meter and falls slowly as compared to the increase at the entry length for another meter of the reactor length, then again gradually increases at the end of the reactor length. A similar trend was observed for other ratios of H_2:CO_2 with an increment of 0.2 in the hydrogen composition at the inlet.

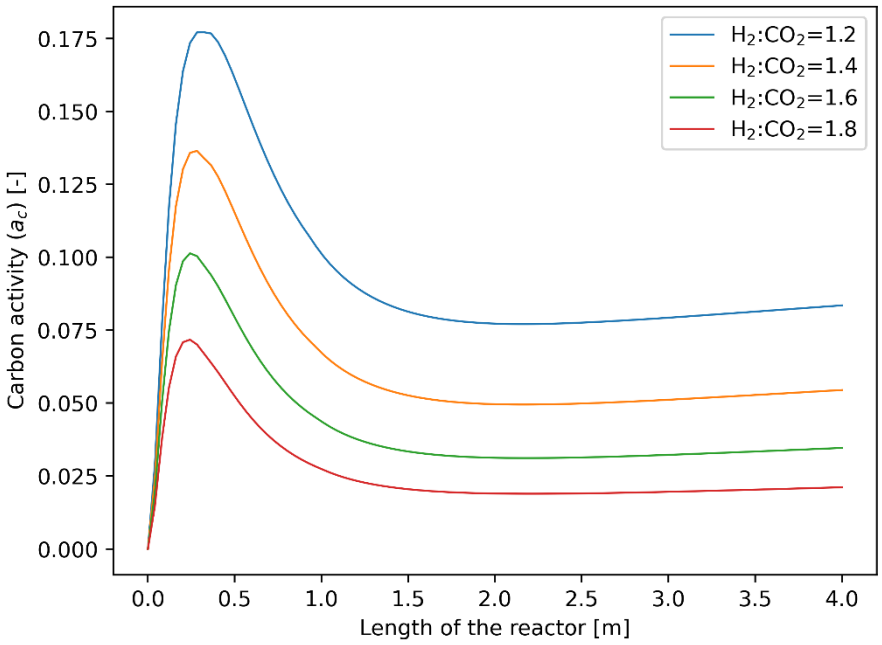

Fig. 16 Carbon activity calculated (Table 6) based on the reaction quiotient and equilibrium constant to determine carbon formation along the length of the reactor for increasing H_2:CO_2 composition. Since the carbon activity is less than 1 for all ratios of H_2:CO_2 there are no carbon formation is the tubula reactor for the operating conditions given in table 3.

The rapid increase in carbon formation potential is because of the partial pressure of CO increasing at the inlet of the reactor from zero, also the equilibrium quotient is calculated as partial pressure of carbon dioxide divided by square of carbon monoxide's partial pressure. When squared, partial pressure of CO produces a very small number and when used to divide partial pressure of CO_2 the equilibrium quotient becomes large. Parallelly, the equilibrium constant of boudouard reaction decreases exponential as the temperature increases from 923K to 1098K therefore causing a rapid increase in carbon formation cause a steep peak. The increase in carbon activity is due to the effect of temperature on boudouard reaction. The carbon activity is well below 1, signifying no net carbon formation. But the composition of CO at the inlet eventhough small, results in a very minimal chance of carbon activity at inlet temperature (923K). This carbon activity can be decreased significantly for increasing the H_2:CO_2 ratios as show in Fig. 16. The carbon activity peak at entrace for H_2:CO_2 = 1 is negligible compared to H_2:CO_2 = 1.8.

In Fig. 16, once the peak in carbon activity is attained, the temperature of the reactor is 1098K after which the equilibrium constant and the partial pressure of CO stops to increase exponentially therefore causing a decrease in the carbon activity. The decrease in equilibrium constant K is slow since the heat transfer is slow compared to the kinetics of the reaction. The temperature increases after 1 meter of the reactor neglibible and the reactor acts isothermally. Also, the rate of increase in partial pressure of CO is slow as compared to the initial reactor length where the kinetics was fast. This is observed in Fig.11 were the concentration of CO_2 increases exponentially at the beginning of the reactor and reaches equilibrium, then only negligible change in CO_2 or CO concentration is observed.

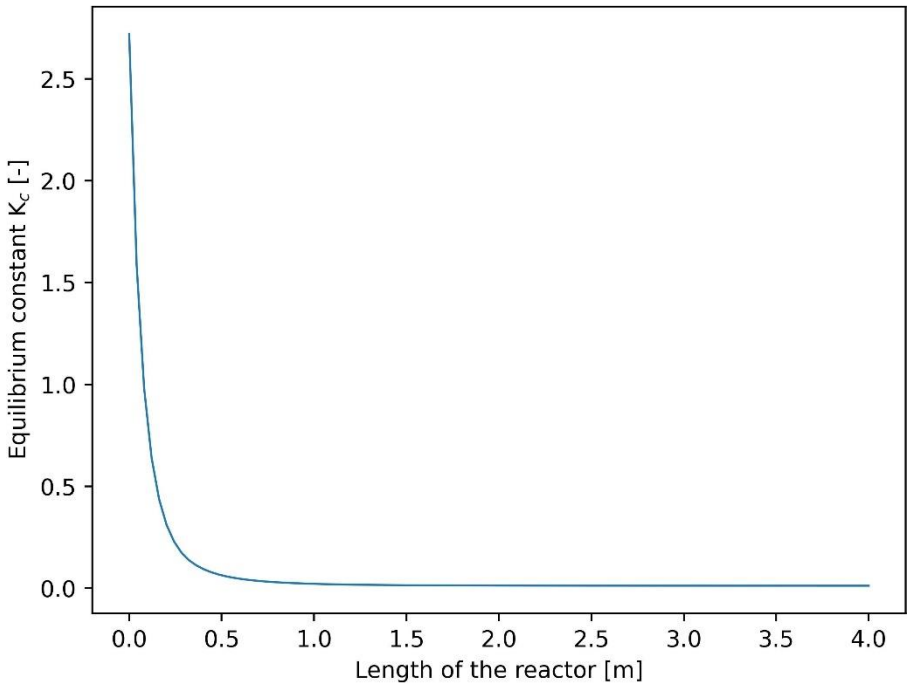

Fig. 17. The equilibrium constant of bouduard reaction along the length of the reactor showing significnat decrease as the temperature in the reactor raises. K_c *becoming almost zero after 1 meter were the reactor temperature reaches its maximum after which only negligible change in observed in temperature subsequently* K_c*. Signifying formation of CO is favoured instead of carbon and* CO_2

For all ratios of H_2:CO_2 the carbon formation decreases since the partial pressure of H_2 in the system increases therefore reducing the overall partial pressures of CO and CO_2 in the reactor. Therefore, reducing the carbon activity in the boudouard reaction, the carbon activity for all ratios of interest are well below 1 signifying that no carbon formation will occur at any length of the reactor for these operating conditions.

Considering there will never be a full conversion, there are certainty for the outlet stream end up with a certain recycle flow. Subsequently there might also be some other components in the feed such as H_2O and CO in the recycle stream their effect in the inlet on carbon formation should be well understood. Therefore, H_2O and CO are considered in the inlet of the reactor to observe their effects.

Table 7 : operating conditions used to observe the effects of H_2O *& CO in the feed on carbon formation.*

GHSV	6000 h^{-1}
T_{wall}	950°C
T_{inlet}	650°C
H_2:CO_2	1.6

Effects of H_2O in the feed :

For the above-mentioned conditions, the peak carbon activity is 0.057055 observed at the initial stage of the reactor around 0.5 m. The H_2:CO ratio of 2.0472 and outlet temperature of 948^oC satisfies required outlet conditions. When the inlet feed consisted of 1% H_2O and rest H_2,CO_2, no significant change in carbon activity is observed. The carbon activity peak shifted from 0.057055 to 0.05743. The amount of H_2O in the feed is increased to 5% with a similar H_2:CO_2 ratio as before, the added H_2O showed high influence on decreases the carbon activity. The carbon activity decreased from 0.057055 to 0.04601 respectively. This is because of H_2O decreasing the partial pressure of CO_2 and CO in the reactor entry as compared to conditions without H_2O. For the 5% H_2O case, the composition of syngas at the outlet of the reactor also varied increasing the ratio from 2.0477 to 2.1908 for 2 meters length of the reactor. If the H_2:CO_2 ratio is decreased from 1.6 to 1.4, with 5% of H_2O in the feed, the outlet composition is attained, but the carbon activity increased from 0.057053 to 0.06773. Therefore, the influence of H_2O in the feed allows decreasing carbon activity but aid in lower conversion of CO_2 thus either wall temperature or the inlet gas temperature needs to be varied to get the same conversion when no H_2O was present in the system.

Effects of CO in the feed :

Firstly, a feed consisting of 1% CO rest H_2 and CO_2 is used as the inlet composition, the carbon activity peak shifted significantly from 0.057055 to 0.7843. Indicating high affinity for carbon formation at the inlet of the reactor. Since the partial pressure of CO is higher as compared to no CO in the inlet feed therefore, the affinity to form carbon is more. Similarly for 5% of CO in the inlet, overshoots the peak carbon activity beyond 1 at the inlet of the reactor. As noted from previous observations, H_2 in the feed has more influence on reducing carbon activity as compared to H_2O. Secondly, carbon activity for 2% CO rest H_2, CO_2 with 2.5:1 ratio is used a feed, the carbon activity reduced from 0.7843 to 0.2242 but the composition of syngas (H_2:CO) at the outlet increased to 2.558. Hence, more CO recycles are required to attain the syngas composition for downstream FT synthesis reflecting inefficiency and risk for carbon formation. Finally, 5% CO with H_2:CO_2 of 2.5 resulted in peak carbon activity of 0.498, but outlet syngas composition was only 2.255. High H_2:CO_2 ratios are not used due to higher composition of H_2 in the syngas, required composition of syngas can't be attained if CO is available at the inlet for operating condition mentioned in Table 7. The suitability for carbon formation at the initial part of the reactor is high as the composition of CO in the inlet feed increase.

4.3.2 Temperature

RWGS is an endothermic reaction therefore, it requires heat input to convert CO_2 and H_2. Similarly undesired side products such as methane and carbon are formed at lower temperatures [20,21], the influence of temperature is also exhibited on the reaction rate, since the reaction rate increases as a function of temperature according to the Arrhenius equation. Therefore, temperature plays a vital role in determining the reactions that runs inside the tubular reactor and the rate in which they proceed. Operating parameters regards to temperature are the inlet gas temperature and the wall heat input for running the endothermic RWGS.

4.3.2.1 Inlet temperature

Inlet gas temperature is critical with regards to carbon formation and methanation in the system, since boudouard is favored at lower temperature < 450^{o}C [16,19]. According to literatures to avoid their occurrences in the initial part of the reactor the inlet gas temperature should be maintained above 450^{o}C for an equimolar inlet feed of only CO_2 and H_2. But the impact of inlet temperature on outlet conditions such as the composition and outlet feed temperature are unavailable in literatures for inlet compositions other than equimolar. Therefore, inlet temperature is varied from 350^{o}C to 650^{o}C to determine the effect of inlet temperature on carbon formation and methane formation, also keeping in mind the desired outlet conditions.

The inlet composition and wall temperature are fixed to 1.6 and 950^{o}C respectively, for a space velocity of 6000 h^{-1} resulting in 2-meter length of the reactor. When the reactor temperature is at 350^{o}C, carbon formation was observed at the initial length of the reactor at 0.101 meter with a carbon activity of 2.19. Next, the inlet temperature was increased to 450^{o}C, resulting in a significant decrease in carbon activity from 2.19 to 0.49. Implying above 450^{o}C carbon formation at the inlet can be avoided with a larger buffer as compared to equimolar inlet composition. As the inlet temperature increased, to 550^{o}C the carbon activity decreased furthermore for the same inlet composition but resulting in more conversion of CO_2. The syngas composition (H_2:CO) decreases as the inlet temperature increases, since higher conversion of CO_2 is achieved and produced more CO. Therefore, less to no methane was produced, at all temperature ranges. Methane was observed at 2.8% of the entire outlet feed composition for an inlet temperature of 650^{o}C, increasing the temperature resulted in more methane formation since availably of CO is high at the end of the reactor. Higher the inlet temperature carbon formation is suppressed, and methane formation is minimized at the initial reactor length.

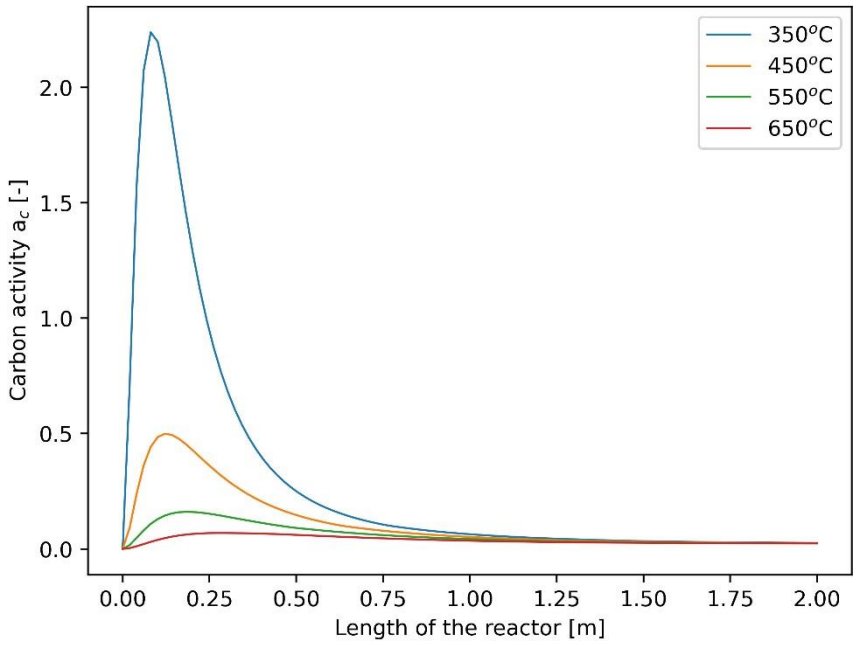

Fig. 18 Carbon activity (a_c) along the length of the tubular reactor with varying inlet temperature to determine the effect of inlet temperature on carbon activity for H_2:CO_2 = 1.6, T_{wall} = 950°C, GHSV = 6000 h^{-1} and 20 bar pressure.

4.3.2.2 Wall temperature

The fixed wall temperature determines the rate of reaction in the tubular reactor due to the endothermicity of RWGS, and the conversion of CO_2 along the length of the reactor. More importantly, wall temperature influences the outlet temperature of the reactor, that needs to be in range with the desired outlet temperature for downstream FT synthesis. Fig 19 shows the temperature profile along the length of the reactor for varying wall temperature.

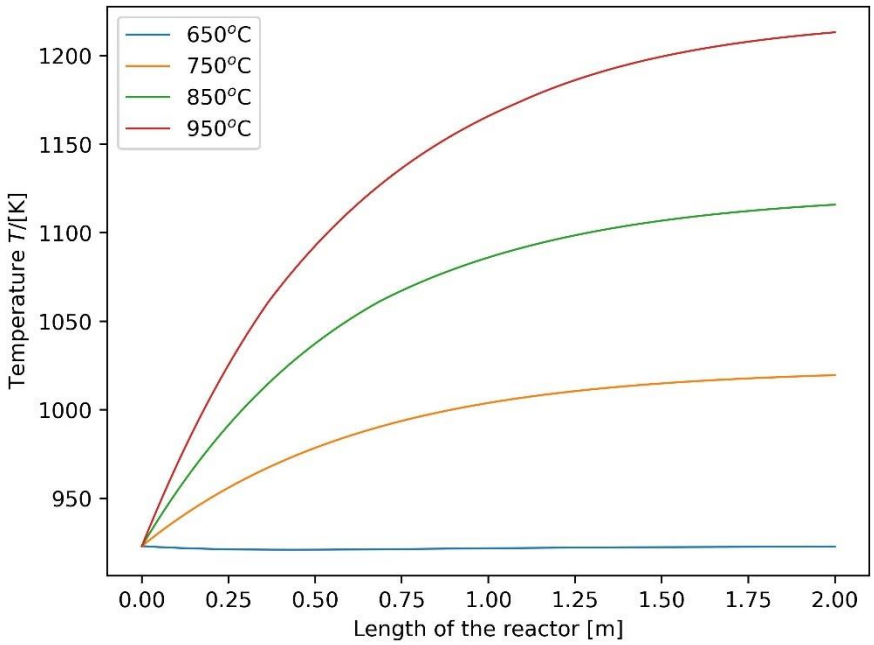

Fig. 19 Axial temperature profile along the length of the tubular reactor for H_2:CO_2 = 1.8, T_{inlet} = 650°C, GHSV = 6000 h^{-1} and 20 bar pressure.

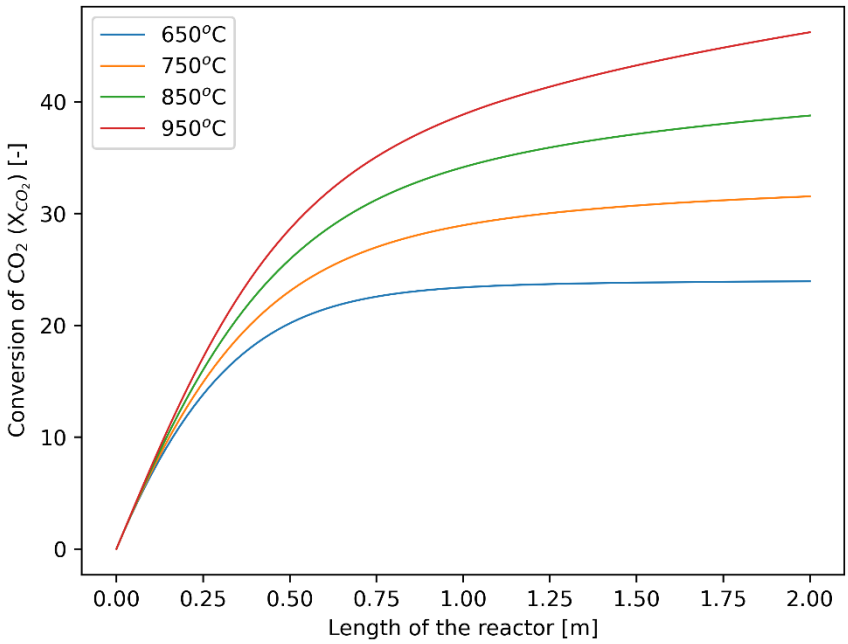

Fig. 20 Conversion of CO_2 along the length of the tubular reactor with varying fixed wall temperatures for H_2:CO_2 = 1.8, T_{inlet} = 650°C, GHSV = 6000 h^{-1} and 20 bar pressure.

During the initial modelling phase, reactor length was kept as 6 meters, with a space velocity of 3000 h^{-1} the kinetics was faster as compared to the heat transfer for the first 2 meters of the reactor. The remaining 4 meters was ideal or close to equilibrium with negligible change in composition. Thus, the GHSV was increased from 3000 h^{-1} to 6000 h^{-1} resulting in a reactor with less catalyst volume and attaining required outlet syngas composition. Longer reactor length is needed only to attain the desired outlet temperature since heat transfer is limited. To counter this problem in a short reactor, desired outlet temperature is attained by increasing the fixed wall temperature. The wall temperature increases along the length of the reactor if the wall temperature is greater than the inlet temperature. For a wall temperature equal to the inlet temperature, the reactor acts isothermally. The desired outlet temperature of the reactor for downstream FT synthesis is 850 – 950°C. If the wall temperature is at 850°C, an outlet temperature of 838°C is attained with a syngas composition of 2.67 for a H_2:CO_2 of 1.6, GHSV of 6000 h^{-1}, inlet temperature of 650°C and 2 meters reactor length. The obtained syngas composition and outlet temperature is undesired. Therefore, to increase the conversion of CO_2 or production of more CO the wall temperature is increased to 950°C for the same above-mentioned conditions. The outlet temperature obtained is 936°C, with an outlet syngas composition of 1.88453.

The wall temperature brings us to one of the objects to determine the heat input required for the tubular reactor. The heat flow to the reactor is given in terms of the overall heat transfer coefficient (U) calculated to be 850 W/m^2 K , the heat exchanger area (A) for the reactor is 0.27935 m^2 for a 2-meter-long reactor with inner tube diameter of 0.04446, and the temperature difference between the fixed wall of 950°C and the reactor temperature. The heat added to the reactor for getting the desired outlet conditions is 60 kW. It is observed from (Fig.19) the conversion CO_2 increased with increase in wall temperature signifying the reaction is heat transfer limited and not kinetically limited.

The impact of wall temperature is significantly more as compared to the impact of inlet temperature on the conversion of CO_2 and attaining the required syngas composition.

4.3.3 Pressure

The allowable pressure drop for the tubular reactor without compromise in operating costs are 1 bar. The operating pressure of the tubular reactor is 20 bar, the pressure drop is calculated according to the Ergun's equation mentioned in chapter 4 and estimated depending on the superficial velocity at the inlet. The superficial velocity determines the residence time in the reactor, for higher conversion the residence time is more compared to lower conversion. For a particle size of 5 mm, the pressure drop per meter length of reactor is plotted against the superficial velocity to determine the maximum superficial velocity above which the pressure drop exceeded the allowable 1 bar.

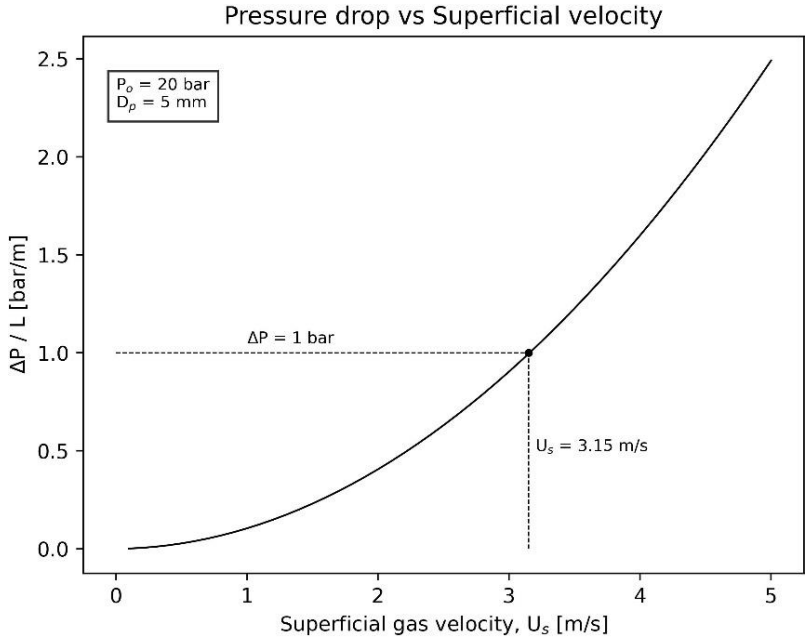

Fig. 21 Pressure drop per meter length calculated using the Erguns equation (Eq. 45) for varying superficial velocities for the operating conditions at H_2:CO_2 = 1, T_{inlet} = 650°C, T_{wall} = 650°C, GHSV = 3000 h^{-1} and 20 bar pressure, used to determine the maximum superficial gas velocity for an allowable pressure drop of 1 bar.

For lower superficial velocities, the pressure drop is very less, as the superficial velocity increases, the pressure drop per meter length of the reactor increases steeply. The pressure drop of the reactor for a superficial velocity of 3.15 m/s is 1 bar that is the allowable pressure drop in the system. This velocity is the maximum allowable superficial velocity and subsequently the gas hourly space velocity can be calculated. In cases when the reactor length is more than 1 meter, then the maximum allowable superficial velocity is below 3.15 m/s. Allowing higher residence time and increased conversion that might result different composition at the outlet than desired.

For the reactor sizing used in the model, for space velocity of 6000 h^{-1} and length of 2 meters, the superficial velocity U_s is 2.1 m/s. Therefore the pressure drop for the system is 0.413 bar/m length of reactor, thus when the reactor length is 2 meter the

maximum pressure drop according to the ergun equation is 0.826 bar that is less than the allowable pressure drop assumed for the tubular reactor. Therefore the conditions in the reactor does not result in pressure drop greater than 1. The pressure drop is also dependent on the particle diameter, the size of the particle or the catalyst diameter controls the flow of fluid along the length of the reactor, when the particle size is small, the pressure drop in the reactor is high due to resistance due to the packed particles in the bed, compared to larger particle size. The pressure is evaluated for different particle diameter at varying superficial velocities, to illustrate the effect of particle size on the pressure drop.

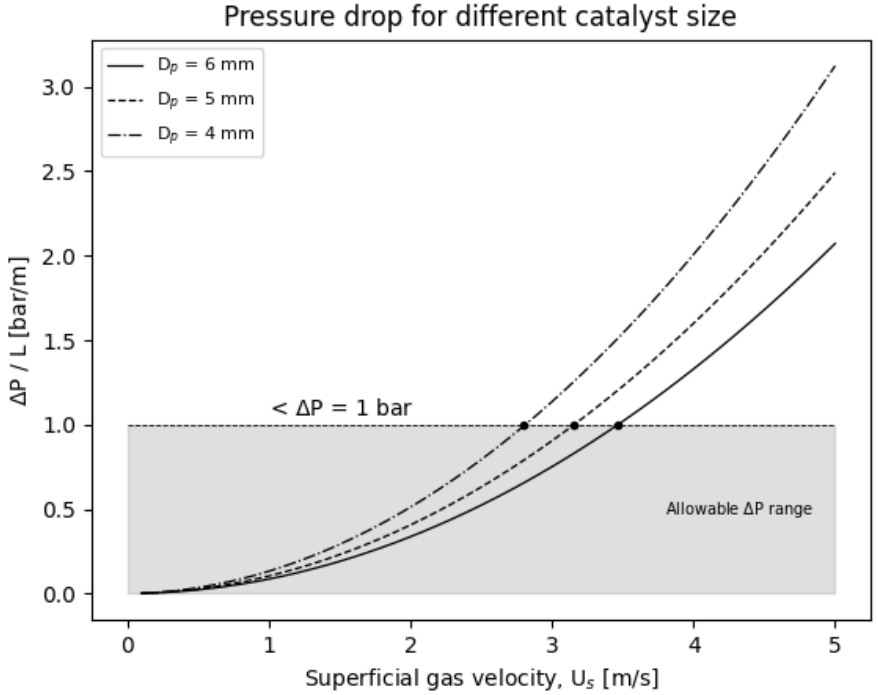

Fig. 22 : Influence of particle size on pressure drop per meter length calculated using the Erguns equation (Eq. 45) for varying superficial velocities for the operating conditions as in Fig.21. The allowable pressure drop for the system is set to be at 1 bar/m above which either particle size or superficial velocity needs to be varied to attain the pressure drop limit. Attainable superficial velocities increases with increasing particle size for an allowable pressure drop of 1 bar.

At very low superficial velocities that pressure drop in the tubular reactor for varying catalyst particle size are non-distinguishable. After the superficial velocity increase above 1 m/s the distinction between 6 mm, 5 mm and 4 mm are evident, as the superficial velocity increases the pressure drop for 6 mm size particle as expected before produces a larger pressure drop as compared to the other smaller particle sizes. The maximum allowable superficial velocity for 1 bar of pressure drop per meter length of reactor also decreases as the catalyst particle size decreases. Therefore, particle size is an important parameter for investigation in the future regards to pressure drop.

The equilibrium composition of gases are evaluated at varying pressures using gibbs minimization method that provides thermodynamic equilibrium composition of gases at given operating conditions. Using the gibbs minimization method the variation in composition at pressures 10 bar and 30 bar are shown in Fig.22. The equilibrium

compositions at these pressures illustrates the achievable composition at given temperature for an equimolar inlet composition of feed with only H_2 and CO_2.

Importantly the methane composition increases with the increase in operating pressure, on the contrary CO composition decrease with increase in operating pressure from 10 bar to 30 bar. This following is observed since, the partial pressure of the gaseous reactants are is increased, the equilibrium shifs towards producing CH_4 and H_2O via the CO hydrogenation reaction. Since the products has less number of gaseous molecules compared to CO and H_2. The increase in CH_4 composition is the range of 5 – 7% for temperatures between 750 and 1000^{o}C. There are only 1– 2 % decrease in CO composition, at the similar operating temperature. The equilibrium composition of H_2 is less at 30 bar as compared to 10 bar, the difference increases steadily between 750 and 1000^{o}C then decreases to reach a 2% difference in equilibrium composition at higher temperatures. There reactor operates between 650 – 950^{o}C, notable changes in the compositions are observed at this temperature range between 10 bar and 30 bar pressure. The downstream operating pressure of Fischer-Tropsch synthesis is between 20 – 40 bars for H_2:CO = 1.7 – 2.15 to produce liquid fuels in a fluidized or slurry reactor with Cobalt or iron catalyst [82]. Therefore economically, using higher operating pressure is preferred over operating at atmospheric conditions, considering downstream FT synthesis. But the reactor is prone to methane compared to operating at lower pressures, therefore using appropriate temperature at the inlet to minimize methane at high operating pressure.

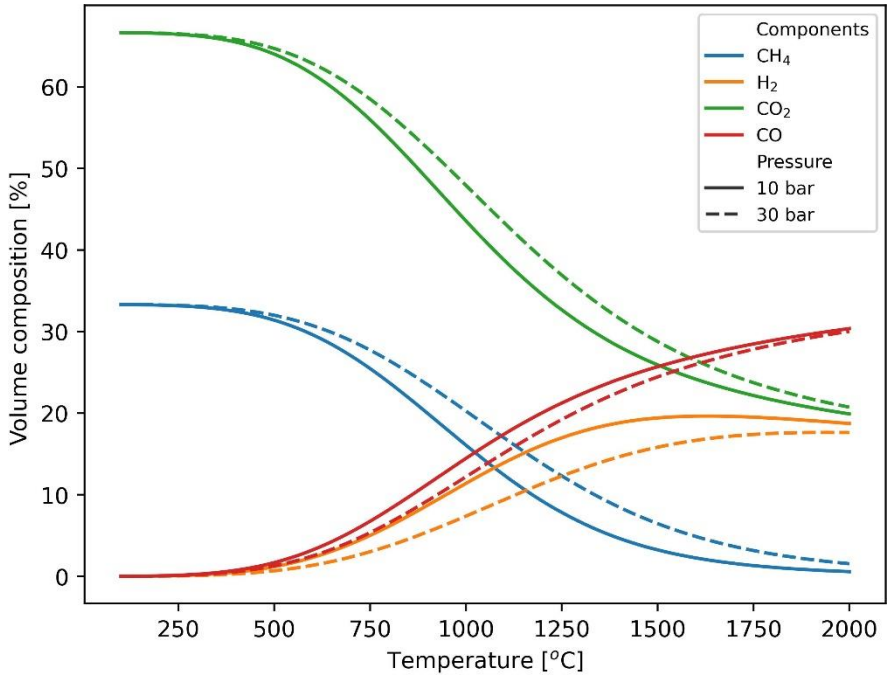

Fig. 23 Influence of pressure on the equilibrium composition of components in the system calculated using the Gibbs minimization method, composition of CH_4 increases with increase in temperature and the composition of CO decreases with increase in pressure for similar temperatures.[2]

[2] Composition of CO and H_2O overlaps each other therefore not plotted in the above graph.

Conclusion and Recommendations | 5

5.1 Conclusion

Motivation and background of work: This work aim is using CO_2 as an abundant raw material produced by human activities. The carbon capture and storage are one part of preventing environmental impacts due to CO_2, but utilization of stored CO_2 is necessary. Hence, there is a considerable need for research on utilization of CO_2, in this work the focus is towards producing useful chemicals specifically heavier hydrocarbons. CO_2 as raw material liquid fuels can be produced by the following steps:

1. Use efficient system for separating CO_2 from effluent gas, streams or capture CO_2 from air using Direct air capture technology.
2. Produce H_2 with alkaline water electrolysis or newer technologies such as includes polymer electrolyte membranes (PEM), Solid oxide electrolyzes (SOEC), and carbon-assisted water electrolysis (CAWE) with electricity from renewable sources.
3. Conversion of CO_2 and H_2 to CO via Reverse water gas shift (RWGS); and produce synthetic gas with CO and renewable H_2.
4. Finally, use the renewable synthetic gas to hydrocarbons or liquid fuels via Fischer Tropsch (FT) synthesis.

Focus is on high temperature RWGS to produce syngas using Ni based catalyst. The formation of carbon that deactivates the Nickel catalyst and reduces the effectiveness of the catalyst. Additionally, methane is an undesired product that is produced as a by-product of side reaction when CO is produced in the tubular reactor. These two challenges are addressed in this work to achieve an efficient first step in producing liquid fuels.

Outline of model: A plug flow tubular reactor was modelled in python to determine the composition and the temperature profile to a reasonable extent. The primary derivation from the concentration and temperature profile is to identify the heat input, space velocity, pressure, temperature required to achieve the desired conversion at the outlet for a reverse water gas shift tubular reactor. So that, the composition at the reactor exit is useful for downstream FT synthesis. The secondary objective is using the concentration along the reactor length to determine operating window for the functioning of the reactor without carbon formation and minimizing methanation. The catalyst is modelled incorporating the internal and external mass transfer limitations. The focus is on carbon formation for a specific Ni based catalyst of interest. Ni based catalysts are found to be more prone to carbon formation as compared to expensive noble metal catalysts. Alternatively, Ni is widely available and inexpensive therefore are of keen interest. In practice full conversion

is never achieved, recycling of outflow is necessary. Subsequently some components might end up in the recycled inlet feed and their effects on the outlet composition and carbon formation are studied by adding H_2O and CO in the feed.

Conclusion of work :

The main objective was to determine the operating conditions for the RWGS tubular reactor to attain syngas at appropriate composition. The table below provides a summary of the operating parameters and their impact on the reactor.

Table 8 : Summary of input parameters and resulting effects on syngas composition, carbon formation and methanation.

Fixed Input Parameters	
Tube outer diameter, d_o	60.3 mm
Tube wall thickness	2.77 mm
Catalyst size, d_p	≥ 5 mm
Bed Porosity	0.4
Variables	
Tube length, L	2 – 2.5 m
Pressure, P	20 – 25 bar
Space velocity	3000 – 6000 h^{-1}
Inlet temperature, T_i	≥ 600°C
Wall temperature, T_w	≥ 950° C
Output Parameters	
H_2:CO_2	1.4 – 1.8
H_2:CO	1.8 – 2.1
Outlet temperature, T_{out}	> 900°C
Peak carbon activity, a_c [1]	0.05 > a_c > 0.29
Methane reactor outlet [vol %] [2]	< 5 %

[1] Range of peak carbon activity for given operating conditions above

[2] Methane formation for the above operating conditions was always lower than 5 % of total outlet volume composition.

The reactor was more prone to carbon formation at the initial length of the reactor around 0 to 0.7 meter. The potential for carbon formation increased at the entry of the reactor because off two reasons, the temperature at the entry of the reactor and the partial pressure of CO at the entry. At initial lengths, the reactor attains a maximum value of carbon activity, after which it drop exponentially when the temperature along the reactor increases and becomes negligibly small. The carbon activity is greater than 1 for feeds consisting only H_2 and CO_2 in ratio 1 > H_2:CO_2 > 2 and inlet temperature of 350°C to 550°C with wall temperature of 950°C, signifiying carbon formation. The peak carbon activity at the initial reactor length become insignificant (<< 1) at inlet temperature > 600°C. Also methane formation at the outlet for H_2:CO_2 > 2 is higher compared to H_2:CO_2 < 2. For H_2:CO_2 = 1.6; 4% of methane was observed of total outlet volume compared to

11.4% for H_2:CO_2 = 2.5. Depending on the composition of H_2 and CO_2 in the feed, the inlet temperature is varied for lowering the carbon activity at the initial reactor length. Increasing the inlet temperature had less effect on methane formation compared to H_2:CO_2 ratio. Therefore it is found increasing the inlet temperature > 600^{o}C results in lowering or eliminating the possibililty of carbon formation and inlet composition H_2:CO_2 < 2 resulted in minimizing methane at the reactor outlet below 5% of the total outlet feed. At higher ratios of H_2:CO_2, CO hydrogenation converts produced CO to CH_4 resulting in higher formation of methane in the system because excess unreacted H_2 reacts with CO to produce CH_4. The effect of H_2:CO_2 ratio also played a vitial role in decreasing carbon activity. The increases in H_2 in the feed, decreases the partial pressure of CO and decreases carbon activity. Compared to equimolar inlet composition, when H_2:CO_2=1.6 carbon activity dropped by 4 times for inlet temperature of 650^{o}C. For H_2:CO_2 ratios > 2 the composition of syngas required for downstream Fischer Tropsch reactor is not achieved. For an outlet temperature of 938^{o}C, desired H_2:CO ratio between 1.8 – 2 is obtained, therefore an appropriate wall temperature is given as ≥ 950^{o}C to reach the desired outlet conditions. Therefore the reaction is heat transfer limited, kinetics are fast allowing high space velocity of 6000 h^{-1} compared to 3000 h^{-1} that was used for initial model estimates. At space velocity of 6000 h^{-1} the reactor produced identical conversion with lower catalyst volume.

Increasing the inlet temperature results in lesser carbon formation and helps in attaining the desired reactor outlet temperature with short reactor length. Increasing the H_2:CO_2 ratio decreases the carbon formation but increases methane formation and increases the composition of H_2 in syngas. Increase in wall temperature increases conversion and aids in attaining the desired syngas composition and outlet temperature. Adding H_2O in the feed aids in lowering carbon formation and varies the outlet composition of syngas. If the recycled inlet feed consists of CO the affinity for carbon formation is very strong. The operating pressure has low impact on reverse water gas shift, increasing the pressure increases attainable equillibrum composition of methane but are below the allowable range at the reactor outlet. Operating at higher pressure is pressure is favorable since Fischer Tropsch synthesis operates at pressure between 20-40 bar it is advised to use similar high pressure of 20 bar to operate the RWGS tubular reactor since pressure has less influence on the system, therefore pressure between 20 – 25 bar is advised.

The operating window for eliminating carbon formation is a inlet temperature > 600^{o}C, H_2:CO_2 between 1 and 2, with a wall temperature of > 950^{o}C and a space velocity of 6000 h^{-1}. For mentioned reactor conditions a length of 2 meters is calculated based on the space velocity that results in a pressure drop of 0.63 bar that is less than allowable pressure drop of 1 bar. The outlet conditions are, syngas ratio (H_2:CO) of 1.85 – 2.1 depending on the combination of inlet temperature, wall temperature and inlet H_2:CO_2 ratio. For H_2:CO_2 = 1.6, T_{wall} = 950^{o}C, T_{inlet} = 650^{o}C, P = 20 bar pressure, GHSV = 6000 h^{-1}, Length = 2 meters, the outlet condition are T_{out} = 938^{o}C, syngas ratio (H_2:CO) = 1.94, with peak carbon activity of 0.005 << 1 signifying no net carbon formation and methane composition at outlet 4% minimal compared to other inlet conditions.

5.2 Recommendations for future research

The thesis, combines both process and chemical engineering, highlighting interesting approaches for exploitation of CO_2. In this section recommendations are given for further research and improvement of the model. A tubular plug flow reactor has been modelled in this thesis, for evaluating carbon formation and methanation for a specific catalyst.

1. Perform experiments to determine the accuracy of the python model, even though the model is validated using the equilibrium constants. Experimental validation should be used to finetune and improve the model.

2. Currently the heat input in a constant of the reactor. The heat input can be varied along the length of the reactor to effectively reduce the heat input required to run the reactor and possibly increase conversion by varying the wall temperature at heat transfer limiting areas in the reactor.

3. Momentum balance should be included to the model since for reactor lengths greater than 2 meters. The pressure drop for longer reactor would be greater than 1 bar, resulting decrease in conversion and increase in operational cost. Therefore required syngas composition might not be obtained.

4. Most of the kinetic data available in literatures for Ni based catalyst are for stream methane reforming purposes, a pathway for future research would be to experimentally determine kinetic rates specifically focusing on, methantion and carbon formation explicitly for Ni catalysts at varying operating conditions. After that carbon formation can be assessed in terms of quantitatively instead of qualitatively.

5. Investigation on direct CO_2 to liquid fuels synthesis, a new path to carbon capture and utilization by direct CO_2 the direct method uses a single reactor with carbon dioxide as its feed, the reactor combines both RWGS and FT reactions to produce lighter hydrocarbons. The overall reaction is exothermic, providing an energy advantage over RWGS, but designing a catalyst with water resistance and high selectivity of olefins selectivity is challenging.

APPENDIX | A

A1 verification of assumptions

A.1.1 Plug flow condition

The plug flow condition is validated using the following conditions, where L is the length of the tubular reactor bed, d_p is the catalyst particle diameter, and d_b is the diameter of the catalyst bed. [83]

$$\frac{L}{d_p} > 40$$

$$\frac{d_b}{d_p} > 10$$

The tubular reactor is assumed to have a length of 2 m with diameter of 0.055 m and for catalyst particle diameter of 5 mm. The above equations are satisfied to indicate the reactor operates in ideal plug flow condition.

A.1.2 Radial temperature gradient

The one-dimensional model is adequate for initial reactor design and observe the effects of process parameters, but the Mears criteria used to identify the effects of radial temperature gradient in the system, [83]

$$\frac{|\Delta_r H|\, r_a\, (1-\varepsilon_b)\, (1-b)\, d_t^2\, E_a}{\lambda_{er}\, T_w} < \frac{1.6\, R\, T_w}{1 + 8\frac{d_p}{d_t\, Bi_w}}$$

$$\mathrm{Bi_w} = \frac{h_w\, d_p}{\lambda_{er}}$$

and,

$$h_w = 0.504\ Re^{0.67}\ Pr^{0.40} \left(\frac{k}{d_p}\right)\left(\frac{d_p}{d_{\text{tube,inner}}}\right)^{0.375}$$

Were,

$\Delta_r H$	Enthalpy of reaction	J mol^{-1}
r_a	Reaction rate of limiting reactant	mol kg$^{-1}_{cat}$ s^{-1}
ε_b	Porosity of bed	-
$1-b$	Catalyst pellet fraction of the bed	-
d_t	Tube diameter	m
λ_{er}	Effective thermal conductivity of bed	W m^{-1} K^{-1}
d_p	Particle diameter	m
T_w	wall temperature	K
R	Gas constant	J mol^{-1} K^{-1}
E_a	Activation energy	J mol^{-1}
Bi_w	Biot number for the reactor wall	-
h_w	Heat transfer coefficient of wall	W m^{-2} K^{-1}
k	Thermal conductivity	W m^{-1} K^{-1}

Combining the parameters, calculating the reaction rate for CO_2 as the limiting reactant, evaluating enthalpy of reaction at bulk temperature of the reactor. The left-hand side and right-hand side of the equation comes out to be 0.1364 < 0.2276. Therefore, it is assumed to be no radial temperature gradient in the reactor.

A.1.3 External catalyst surface temperature gradient

The temperature gradient importance at the external catalyst surface can be quantified using the Mears criteria for heat transfer [84].

$$\frac{(-\Delta_r H)\ (-r_a)\ \rho_b\ d_p\ E_a}{h\ T^2\ R} < 0.3$$

The heat transfer between solid and gas *h* is determined using,

$$Nu_{loc} = \frac{\lambda}{h\ d_p} = 3.66$$

Valid when Greatz number is larger than 0.1, The greatz number is calculated by :

$$Gz = \frac{a\ L}{d_p\ u_s}$$

Gz number was determined to be always larger than 0.1 for the operating conditions of the reactor, therefore heat transfer coefficient is calculated using the given Nusselt correlation.

$\Delta_r H$	Enthalpy of reaction	KJ mol^{-1}
r_a	Reaction rate of limiting reactant	kmol kg^{-1}_{cat} s^{-1}
h	Heat transfer coefficient solid & gas	KJ/ m^2 s K
a	Thermal diffusion coefficient	m^2 s^{-1}
L	Length of catalyst bed	m
u_s	Superficial velocity	m s^{-1}

The Mears criteria for heat transfer is calculated using the above-mentioned parameters and is 0.2215 that is less than 0.3. Thus, there is no temperature gradient at the external surface of the catalyst. Furthermore, the thermal conductivity of solid catalyst particle is comparatively higher than the gaseous reaction mixture, in steady state conditions, internal temperature gradients are rarely important in practice [83].

A.1.3 Pressure drop

The allowable pressure drop for the tubular reactor without compromise in operating costs are 1 bar. The operating pressure of the tubular reactor is 20 bar, the pressure drop is calculated according to the Ergun's equation in chapter 4 and estimated to be in the range of 0.1 – 0.5 depending on the superficial velocity at the inlet. For a superficial velocity of 2 m/s the pressure drop is 0.43715 that is 2.1% of the initial operating pressure. The main influence of neglecting the pressure drop are in transport properties like, thermal conductivity, viscosity, and specific heat capacities of the fluid. These properties are determined using PROII Process Engineering 10.2 application for individual components in the tubular reactor. The properties are obtained at operating temperature range of 500 to 1000^{o}C with pressure at 20 bar, similarly for 19 bar assuming a pressure drop of 1 bar.

The obtained set of data compared and variations in properties at 20 bar and 19 bar are determined, finally the error was calculated using the properties at 20 bars as the benchmark. The difference was less than 0.1% for all transport properties.

Table A.1.3: Percentage difference in transport properties for 20 bar and 19 bar.

Property	Difference [%]
Thermal conductivity	0.00783086
Viscosity	0.00267758
Specific heat capacity	0.02053963

From the above table, the pressure drop of 1 bar is a resonably acceptable range since the difference is the transport properties are of negligible magnitude. Therefore pressure drop below 1 bar is assume to be negligible.

A2 Fluid mixture properties

A.2.1 Viscosity

The following semiempirical relation is used for a given gas mixture to predict the viscosity of gas mixture with average deviation of ~ 2 %, [85]

$$\mu_{\text{mix}} = \sum_{i=1}^{n} \frac{y_i\, \mu_i}{\sum\, y_j \phi_{ij}}$$

$$\phi_{ij} = \frac{1}{\sqrt{8}} \left(1 + \frac{M_i}{M_j}\right)^{-1/2} \left[1 + \left(\frac{\mu_i}{\mu_j}\right)^{1/2} \left(\frac{\mu_i}{\mu_j}\right)^{1/4}\right]^2$$

Where ϕ_{ij} is a dimensionless quantity, n is the number of chemical species in a mixture, y_i the mole fraction of species i, μ_i the viscosity of species i at the sytem temperature and pressure, and M_i the molecular weight of species i.

A.2.2 Thermal conductivity

The thermal conductivities for gas mixture k_{mix} is calculated using, [85]

$$\mu_{\text{mix}} = \sum_{i=1}^{n} \frac{x_i\, k_i}{\sum\, y_j \phi_{ij}}$$

Were x_i is the mole fraction of species i and k_i the thermal conductivities of pure gases. The values of ϕ_{ij} are identical to those used to calculate the viscosity of gas mixtures.

A.2.3 Specific heat capacity

The heat capacity of mixture is dependent on the composition and the temperature. The below equation is used to calculate the heat capacity of the mixture. [85]

$$\mathrm{C_{p,mix}} = \sum_{i=1}^{n} y_i \, C_{p,i}$$

The individual heat capacities are determined at operating temperatures according to the Shomate equations for gas phase thermochemistry.

$$\mathrm{C}_{p,i} = A_i + B_i \, t + C_i \, t^2 + D_i \, t^3 + E_i \, t^2$$

Were, A, B,C, D and E are constant of the Shomate equation, t is calculated using below formular where T is in kelvin,

$$t = \frac{T}{1000}$$

APPENDIX | B

B1 Thermodynamic Equilibrium

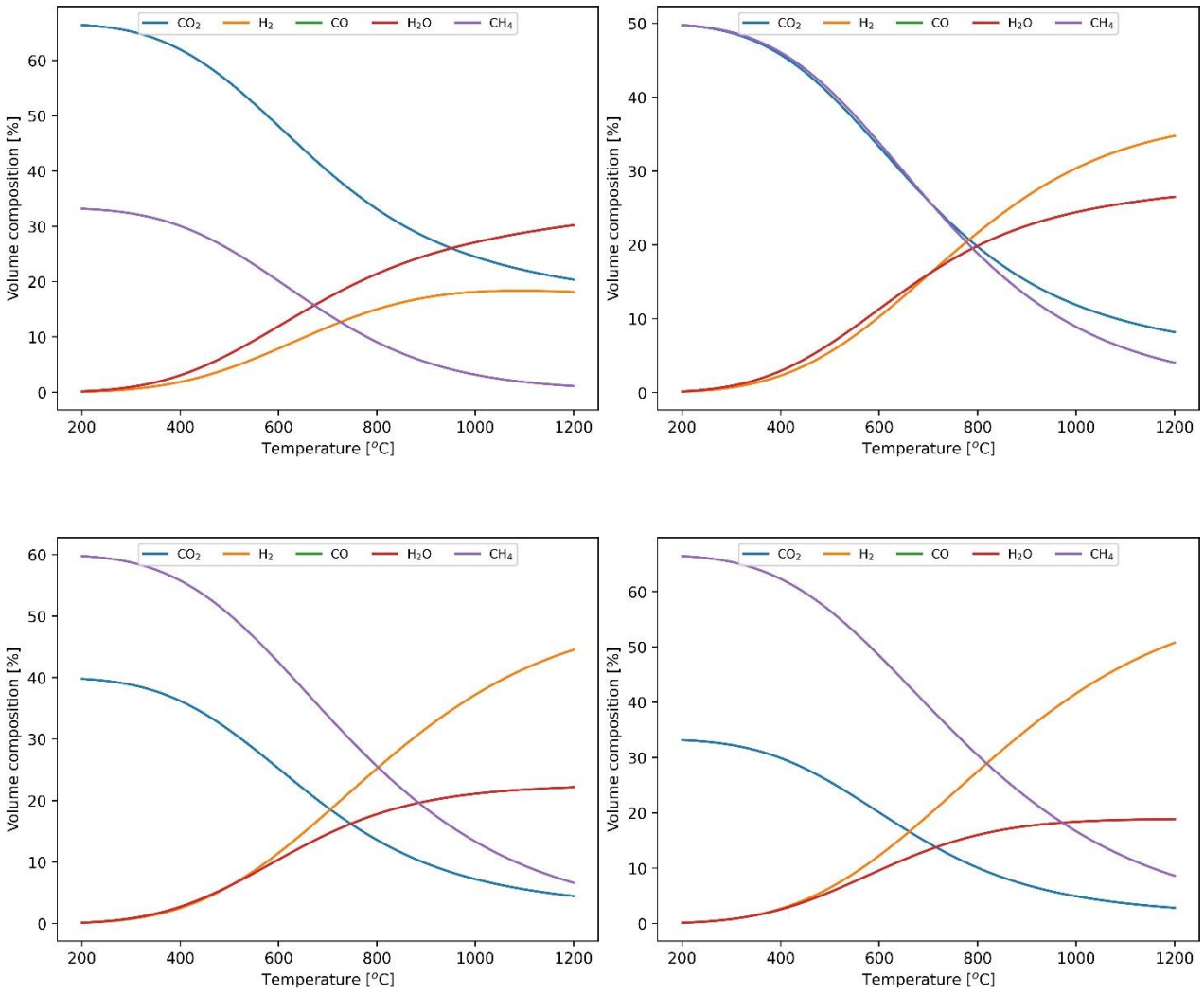

Fig. 24 *Thermodynamic equilibrium composition of components in the reverse water gas shift and methantion reaction at varying temperature at 20 bar pressure and different composition of H_2:CO_2*

B 2 Catalyst properties

Table B.2: Catalyst properties of Ni/Calcium Aluminate used to model the tubular reactor model

Composition	>10% Ni on Calcium Aluminate
Geomentry	Rashig ring (ODx H x ID) (5mm x 5mm x 3mm)
Catalyst Bulk density	950 kg/m^3
Pore volume	0.17 cm^3/g
Average pore diameter	230 nm

Reference

[1] Andrej, F. (2020). Global CO_2 levels reach a new millennial high in 2020, despite the traffic and industry slowdown during the Covid-19 pandemic. Severe weather Europe. https://www.severe-weather.eu/news/global-co2-high-covid-2020-fa/

[2] Global Monitoring Laboratory. (2020). What is the Global Greenhouse Gas Reference Network? Noaa. https://gml.noaa.gov/ccgg/ggrn.php

[3] NASA. (2021). 2021 Tied for 6th Warmest Year in Continued Trend, NASA Analysis Shows. https://www.giss.nasa.gov/research/news/20220113/

[4] Alfons, P.M et al. (2018). Assessment Report. IPCC. https://web.archive.org/web/20181117121314/http:/www.ipcc.ch/pdf/assessment-report/ar4/syr/ar4_syr_appendix.pdf

[5] Rebecca, L. (2020). Climate Change: Atmospheric Carbon Dioxide. https://www.climate.gov/news-features/understanding-climate/climate-change-atmospheric-carbon-dioxide

[6] Zeke, H. (2020). Analysis: When might the world exceed 1.5C and 2C of global warming?, https://www.carbonbrief.org/analysis-when-might-the-world-exceed-1-5c-and-2c-of-global-warming.

[7] NASA's Scientific Visualization Studio (2022). GISTEMP Climate spiral, https://svs.gsfc.nasa.gov/4975.

[8] Dr. Eva, A. (2021). CCS and CCU. Mind explaining what these are again? Neste. https://journeytozerostories.neste.com/circular-economy/ccs-and-ccu-mind-explaining-what-these-are-again#ac87900b

[9] Szulczewski, M. L., MacMinn, C. W., Herzog, H. J., & Juanes, R. (2012). Lifetime of carbon capture and storage as a climate-change mitigation technology. Proceedings of the National Academy of Sciences, 109(14), 5185-5189.

[10] Escobar, W. A. F. (2012). Study of the reverse water-gas shift and dry reforming reactions conditions in a fixed bed reactor.

[11] Centi, G., Quadrelli, E. A., & Perathoner, S. (2013). Catalysis for CO_2 conversion: a key technology for rapid introduction of renewable energy in the value chain of chemical industries. Energy & Environmental Science, 6(6), 1711-1731.

[12] Daza, Y. A., & Kuhn, J. N. (2016). CO_2 conversion by reverse water gas shift catalysis: comparison of catalysts, mechanisms and their consequences for CO_2 conversion to liquid fuels. RSC advances, 6(55), 49675-49691.

[13] Mathew, T., Saju, S., & Raveendran, S. N. (2021). Survey of Heterogeneous Catalysts for the CO_2 Reduction to CO via Reverse Water Gas Shift. Engineering Solutions for CO_2 Conversion, 281-316.

[14] Bahmanpour, A. M., Signorile, M., & Kröcher, O. (2021). Recent progress in syngas production via catalytic CO_2 hydrogenation reaction. Applied Catalysis B: Environmental, 120319.

[15] Lim, H. S., Lee, M., Kim, Y., Kang, D., & Lee, J. W. (2021). Low-temperature CO_2 hydrogenation to CO on Ni-incorporated $LaCoO_3$ perovskite catalysts. International Journal of Hydrogen Energy, 46(29), 15497-15506.

[16] Adelung, S., Maier, S., & Dietrich, R. U. (2021). Impact of the reverse water-gas shift operating conditions on the Power-to-Liquid process efficiency. Sustainable Energy Technologies and Assessments, 43, 100897.

[17] Catalyst Handbook – Chapter 6: Water-gas-Shift Reaction (1996) Edited by Martyn V. Twigg, Second Edition, Manson Publishing

[18] Nikoo, M. K., & Amin, N. A. S. (2011). Thermodynamic analysis of carbon dioxide reforming of methane in view of solid carbon formation. Fuel Processing Technology, 92(3), 678-691.

[19] Wolf, A., Jess, A., & Kern, C. (2016). Syngas Production via Reverse Water-Gas Shift Reaction over a Ni-Al_2O_3 Catalyst: Catalyst Stability, Reaction Kinetics, and Modeling. Chemical Engineering & Technology, 39(6), 1040-1048.

[20] Kaiser, P., Unde, R. B., Kern, C., & Jess, A. (2013). Production of liquid hydrocarbons with CO_2 as carbon source based on reverse water-gas shift and Fischer-Tropsch synthesis. Chemie Ingenieur Technik, 85(4), 489-499.

[21] Aramouni, N. A. K., Zeaiter, J., Kwapinski, W., & Ahmad, M. N. (2017). Thermodynamic analysis of methane dry reforming: Effect of the catalyst particle size on carbon formation. Energy Conversion and Management, 150, 614-622.

[22] Mathew, T., Saju, S., & Raveendran, S. N. (2021). Survey of Heterogeneous Catalysts for the CO_2 Reduction to CO via Reverse Water Gas Shift. Engineering Solutions for CO_2 Conversion, 281-316.

[23] Wang, W., Wang, S., Ma, X., and Gong, J. (2011). Recent advances in catalytic hydrogenation of carbon dioxide. Chem. Soc. Rev. 40: 3703–3727.

[24] Daza, Y.A. and Kuhn, J.N. (2016). CO_2 conversion by reverse water gas shift catalysis: comparison of catalysts, mechanisms and their consequences for CO_2 conversion to liquid fuels. RSC Adv. 6: 49675–49691.

[25] Xu, H., Li, Y., Luo, X. et al. (2017). Monodispersed gold nanoparticles supported on a zirconium-based porous metal–organic framework and their high catalytic ability for the reverse water–gas shift reaction. Chem. Commun. 53: 7953–7956.

[26] Daza, Y. A., & Kuhn, J. N. (2016). CO_2 conversion by reverse water gas shift catalysis: comparison of catalysts, mechanisms and their consequences for CO_2 conversion to liquid fuels. RSC advances, 6(55), 49675-49691.

[27] Sun, F.-M., Yan, C.-F., Wang, Z.-D. et al. (2015). Ni/Ce-Zr-O catalyst for high CO_2 conversion during reverse water gas shift reaction (RWGS). Int. J. Hydrogen Energy 40: 15985–15993.

[28] Unde, R. B. (2012). Kinetics and reaction engineering aspects of syngas production by the heterogeneously catalyzed reverse water gas shift reaction. Universitaet Bayreuth (Germany).

[29] Chen, C. S., Cheng, W. H., & Lin, S. S. (2000). Mechanism of CO formation in reverse water–gas shift reaction over Cu/Al_2O_3 catalyst. Catalysis letters, 68(1), 45-48.

[30] Wang, W., Zhang, Y., Wang, Z., Yan, J. M., Ge, Q., & Liu, C. J. (2016). Reverse water gas shift over In_2O_3–CeO_2 catalysts. Catalysis Today, 259, 402-408.

[31] Zhang, J., An, B., Hong, Y. et al. (2017). Pyrolysis of metal–organic frameworks to hierarchical porous Cu/Zn-nanoparticle @carbon materials for efficient CO_2 hydrogenation. Mater. Chem. Front. 1: 2405–2410

[32] Mutschler, R., Moioli, E., Luo, W. et al. (2018). CO_2 hydrogenation reaction over pristine Fe, Co, Ni, Cu and Al_2O_3 supported Ru: Comparison and determination of the activation energies. J. Catal. 366: 139–149

[33] Liang, B., Duan, H., Su, X. et al. (2017). Promoting role of potassium in the reverse water gas shift reaction on Pt/mullite catalyst. Catal. Today 281: 319–326.

[34] Luhui, W., Hui, L., Yuan, L. et al. (2013). Influence of preparation method on performance of Ni-CeO_2 catalysts for reverse water-gas shift reaction. J. Rare Earths 31: 559–564.

[35] Zhang, Y., Liang, L., Chen, Z., Wen, J., Zhong, W., Zou, S., ... & Ye, D. (2020). Highly efficient Cu/CeO_2-hollow nanospheres catalyst for the reverse water-gas shift reaction: Investigation on the role of oxygen vacancies through in situ UV-Raman and DRIFTS. Applied Surface Science, 516, 146035.

[36] Shen, Y., Xiao, Z., Liu, J., & Wang, Z. (2019). Facile Preparation of Inverse Nanoporous Cr_2O_3/Cu Catalysts for Reverse Water-Gas Shift Reaction. ChemCatChem, 11(22), 5439-5443.

[37] Zhang, X., Zhu, X., Lin, L., Yao, S., Zhang, M., Liu, X., ... & Ma, D. (2017). Highly dispersed copper over β-Mo_2C as an efficient and stable catalyst for the reverse water gas shift (RWGS) reaction. ACS Catalysis, 7(1), 912-918.

[38] Li, S., Xu, Y., Chen, Y., Li, W., Lin, L., Li, M., ... & Ma, D. (2017). Tuning the selectivity of catalytic carbon dioxide hydrogenation over iridium/cerium oxide catalysts with a strong metal–support interaction. Angewandte Chemie, 129(36), 10901-10905.

[39] Chen, C. S., Cheng, W. H., & Lin, S. S. (2001). Enhanced activity and stability of a Cu/SiO_2 catalyst for the reverse water gas shift reaction by an iron promoter. Chemical Communications, (18), 1770-1771.

[40] Chen, C. S., Cheng, W. H., & Lin, S. S. (2004). Study of iron-promoted Cu/SiO_2 catalyst on high temperature reverse water gas shift reaction. Applied Catalysis A: General, 257(1), 97-106.

[41] Kim, D. H., Park, J. L., Park, E. J., Kim, Y. D., & Uhm, S. (2014). Dopant effect of barium zirconate-based perovskite-type catalysts for the intermediate-temperature reverse water gas shift reaction. Acs Catalysis, 4(9), 3117-3122.

[42] Kim, D. H., Han, S. W., Yoon, H. S., & Kim, Y. D. (2015). Reverse water gas shift reaction catalyzed by Fe nanoparticles with high catalytic activity and stability. Journal of Industrial and Engineering Chemistry, 23, 67-71.

[43] Gao, J., Wu, Y., Jia, C. et al. (2016). Controllable synthesis of α–MoC_{1-x} and β–Mo_2C nanowires for highly selective CO_2 reduction to CO. Catal. Commun. 84: 147–150.

[44] Kharaji, A.G., Shariati, A., and Takassi, M.A. (2013). A novel-alumina supported Fe-Mo bimetallic catalyst for reverse water gas shift reaction. Chin. J. Chem. Eng. 21: 1007–1014.

[45] Gonclaves, R.V., Vono, L.L.R., Wojcieszak, R. et al. (2017). Selective hydrogenation of CO_2 into CO on a highly dispersed nickel catalyst obtained by magnetron sputtering deposition: a step towards liquid fuels. Appl. Catal., B 209: 240–246

[46] Ranjbar, A., Irankhah, A., & Aghamiri, S. F. (2019). Catalytic activity of rare earth and alkali metal promoted (Ce, La, Mg, K) Ni/Al_2O_3 nanocatalysts in reverse water gas shift reaction. Research on Chemical Intermediates, 45(10), 5125-5141.

[47] Zhao, K., Bkour, Q., Hou, X. et al. (2018). Reverse water gas shift reaction over CuFe/Al_2O_3 catalyst in solid oxide electrolysis cell. Chem. Eng. J. 336: 20–27.

[48] Luhui, W., Hui, L. I. U., Yuan, L. I. U., Ying, C. H. E. N., & Shuqing, Y. A. N. G. (2013). Effect of precipitants on Ni-CeO_2 catalysts prepared by a co-precipitation method for the reverse water-gas shift reaction. Journal of Rare Earths, 31(10), 969-974.

[49] Lu, B. and Kawamoto, K. (2014). Preparation of mesoporous CeO_2 and monodispersed NiO particles in CeO_2, and enhanced selectivity of NiO/CeO_2 for reverse water gas shift reaction. Mater. Res. Bull. 53: 70–78.

[50] Nityashree, N., Price, C. A. H., Pastor-Perez, L., Manohara, G. V., Garcia, S., Maroto-Valer, M. M., & Reina, T. R. (2020). Carbon stabilized saponite supported transition metal-alloy catalysts for chemical CO_2 utilization via reverse water-gas shift reaction. Applied Catalysis B: Environmental, 261, 118241.

[51] Kim, S. S., Lee, H. H., & Hong, S. C. (2012). A study on the effect of support's reducibility on the reverse water-gas shift reaction over Pt catalysts. Applied Catalysis A: General, 423, 100-107.

[52] Lu, B., & Kawamoto, K. (2013). Preparation of monodispersed NiO particles in SBA-15, and its enhanced selectivity for reverse water gas shift reaction. Journal of Environmental Chemical Engineering, 1(3), 300-309.

[53] R. Zubrin, The Case for Mars, pp. 153, Reverse Water-Gas Shift Reaction - Marspedia

[54] CO_2 Conversion and Utilization: An Overview. Prepr. - Am. Chem. Soc., Div. Pet. Chem. 809 (2002)

[55] Twigg, M. V. (2018). Catalyst handbook. Routledge.

[56] Álvarez, A., Bansode, A., Urakawa, A., Bavykina, A. V., Wezendonk, T. A., Makkee, M., ... & Kapteijn, F. (2017). Challenges in the greener production of formates/formic acid, methanol, and DME by heterogeneously catalyzed CO_2 hydrogenation processes. Chemical reviews, 117(14), 9804-9838.

[57] Parthasarathy, P., & Narayanan, K. S. (2014). Hydrogen production from steam gasification of biomass: influence of process parameters on hydrogen yield–a review. Renewable energy, 66, 570-579.

[58] Inoglu, N. G., & Kitchin, J. R. (2009, March). Adsorbate Cu interactions and catalyst morphologies under reactive water gas shift environment: A first principle study. In abstracts of papers of the american chemical society (vol. 237). 1155 16th st, nw, washington, dc 20036 usa: amer chemical soc.

[59] Forzatti, P., & Lietti, L. (1999). Catalyst deactivation. Catalysis today, 52(2-3), 165-181.

[60] Bartholomew, C. H. (1982). Carbon deposition in steam reforming and methanation. Catalysis Reviews Science and Engineering, 24(1), 67-112.

[61] Marko Subbarao (March 7, 2022), GISTEMP Climate Spiral, NASA's Scientific Visualization Studio, SVS: GISTEMP Climate Spiral (nasa.gov)

[62] Song, C. (2002). CO2 conversion and utilization: an overview.

[63] Fratalocchi, L., Visconti, C. G., Groppi, G., Lietti, L., & Tronconi, E. (2018). Intensifying heat transfer in Fischer-Tropsch tubular reactors through the adoption of conductive packed foams. Chemical Engineering Journal, 349, 829-837.

[64] Szulczewski, M. L., MacMinn, C. W., Herzog, H. J., & Juanes, R. (2012). Lifetime of carbon capture and storage as a climate-change mitigation technology. Proceedings of the National Academy of Sciences, 109(14), 5185-5189.

[65] Deans, H. A., & Lapidus, L. (1960). A computational model for predicting and correlating the behavior of fixed-bed reactors: I. Derivation of model for nonreactive systems. AIChE Journal, 6(4), 656-663.

[66] McGuire, M. L., & Lapidus, L. (1965). On the stability of a detailed packed-bed reactor. AIChE Journal, 11(1), 85-95.

[67] Vanderveen, J. W., Luss, D., & Amundson, N. R. (1968). Stability of adiabatic packed bed reactors. Effect of flow variations and coupling between the particles. AIChE Journal, 14(4), 636-643.

[68] Hill, C. G., & Root, T. W. (2014). Introduction to chemical engineering kinetics and reactor design. John Wiley & Sons.

[69] Iordanidis, A. A. (2002). Mathematical modeling of catalytic fixed bed reactors (pp. 98-112). Enschede, The Netherlands: Twente University Press.

[70] Hlavacek, V. (1977). H., Vortuba, J. Steady-state operation of fixed-bed reactors and monolithic structures. N.-Y, 314.

[71] Xu, J., & Froment, G. F. (1989). Methane steam reforming: II. Diffusional limitations and reactor simulation. AIChE Journal, 35(1), 97-103.

[72] Ertl, G., Knözinger, H., & Weitkamp, J. (Eds.). (1997). Handbook of heterogeneous catalysis (Vol. 2, pp. 427-440). Weinheim: VCH.

[73] Branan, C. R. (1999). Pocket guide to chemical engineering. Elsevier.

[74] PARK∗, I. S., DO, D. D., & RODRIGUES, A. E. (1996). Measurement of the effective diffusivity in porous media by the diffusion cell method. Catalysis Reviews, 38(2), 189-247.

[75] J.M. Zalc, S.C. Reyes and E. Iglesia, The effects of diffusion mechanism and void structure on transport rates and tortuosity factors in complex porous structures. Chem. Eng. Sci. 59 (2004), 2947-2960.

[76] Hayhurst, A. N., & Parmar, M. S. (2002). Measurement of the mass transfer coefficient and Sherwood number for carbon spheres burning in a bubbling fluidized bed. Combustion and flame, 130(4), 361-375.

[77] Moulijn, J. A., van Leeuwen, P. W., & van Santen, R. A. (Eds.). (1993). Catalysis: an integrated approach to homogeneous, heterogeneous, and industrial catalysis. Elsevier.

[78] Froment, G. F., Bischoff, K. B., & De Wilde, J. (1990). Chemical reactor analysis and design (Vol. 2). New York: Wiley.

[79] Ergun, S. (1952). Fluid flow through packed columns. Chem. Eng. Prog., 48, 89-94.

[80] Nield, D. A., & Bejan, A. (2006). Convection in porous media (Vol. 3). New York: springer.

[81] Agüero, A., Baráibar, I., Muelas, R., Oskay, C., Galetz, M., & Korner, E. (2020). Analysis of an aluminide coating on austenitic steel 800HT exposed to metal dusting conditions: Lessons from an industrial hydrogen production plant. International Journal of Pressure Vessels and Piping, 186, 104129.

[82] Gupta, M., & Spivey, J. J. (2013). New and Future Developments in Catalysis: Chapter 5. Catalytic Processes for the Production of Clean Fuels. Elsevier Inc. Chapters.

[83] Moulijn, J. A., van Leeuwen, P. W., & van Santen, R. A. (Eds.). (1993). Catalysis: an integrated approach to homogeneous, heterogeneous and industrial catalysis. Elsevier.

[84] Fogler, H. S., & Fogler, S. H. (1999). Elements of chemical reaction engineering. Pearson Educacion.

[85] Demirel, Y. (2007). Nonequilibrium thermodynamics: transport and rate processes in physical, chemical and biological systems. Elsevier.


TU Delft
T.EN
TECHNIP
ENERGIES